Light-responsive zwitterionic membrane surface modification for antifouling and antibacterial application

Pritam Das, Nadège Durban-Benizio, Sandrine Desclaux, Christel Causserand, Jean-Christophe Remigy, Jean-François Lahitte, Véronique Pimienta, Christophe Coudret, Clémence Coetsier

Journal Pre-proofs

Light-responsive zwitterionic membrane surface modification for antifouling and antibacterial application

Pritam Das, Nadège Durban-Benizio, Sandrine Desclaux, Christel Causserand, Jean-Christophe Remigy, Jean-François Lahitte, Véronique Pimienta, Christophe Coudret, Clémence Coetsier

PII: S1385-8947(24)08828-4
DOI: https://doi.org/10.1016/j.cej.2024.157337
Reference: CEJ 157337

To appear in: *Chemical Engineering Journal*

Received Date: 24 July 2024
Revised Date: 18 October 2024
Accepted Date: 1 November 2024

Please cite this article as: P. Das, N. Durban-Benizio, S. Desclaux, C. Causserand, J-C. Remigy, J-F. Lahitte, V. Pimienta, C. Coudret, C. Coetsier, Light-responsive zwitterionic membrane surface modification for antifouling and antibacterial application, *Chemical Engineering Journal* (2024), doi: https://doi.org/10.1016/j.cej.2024.157337

Light-responsive zwitterionic membrane surface modification for antifouling and antibacterial application

Pritam Das[a,b,c]*, Nadège Durban-Benizio[a], Sandrine Desclaux[a], Christel Causserand[a], Jean-Christophe Remigy[a], Jean-François Lahitte[a], Véronique Pimienta[b], Christophe Coudret[b], Clémence Coetsier[a]*

[a]Laboratoire de Génie Chimique, Université de Toulouse, CNRS, INPT, UPS, F-31062 Toulouse, France

[b]Laboratoire des IMRCP, Université de Toulouse, CNRS UMR 5623, Université Toulouse III—Paul Sabatier, 118 Rte de Narbonne, F-31062 Toulouse Cedex, France

[c]Institute for Infrastructure and Environment, School of Engineering, The University of Edinburgh, The King's Buildings, Edinburgh, EH9 3FG, UK

*Corresponding E-mail: pdas2@ed.ac.uk, clemence.coetsier@univ-tlse3.fr

Keywords: light responsive cleaning, wastewater treatment, azobenzene, zwitterion, antifouling and antibacterial membrane

Abstract

Light-responsive surface modifications offer a promising solution for reducing membrane fouling by enabling remote, contactless cleaning without altering the chemical environment. While traditional methods make membranes hydrophilic to resist fouling, biofouling remains difficult to remove and often requires harsh bactericidal treatments. With the rise of antimicrobial resistance (AMR), there is a pressing need for alternative, non-bactericidal strategies to control biofilm growth. In this study, we developed an efficient approach by coating commercial ultrafiltration polyethersulfone (PES) membranes with a copolymer of light-responsive azobenzene (AZO) and zwitterionic sulphobetaine methacrylate (SBMA). The photochemical conversion efficiency and photokinetic parameters of the copolymer, due to light-induced *trans-cis-trans* conversion, were systematically determined. During filtration, the modified membranes showed excellent resistance to reversible fouling with bovine serum albumin (BSA). The fouled membrane became reusable after near-complete removal of irreversible fouling, including bacteria (*Pseudomonas aeruginosa*), by activating the AZO units with UV-vis light, providing an effective strategy for fouling control.

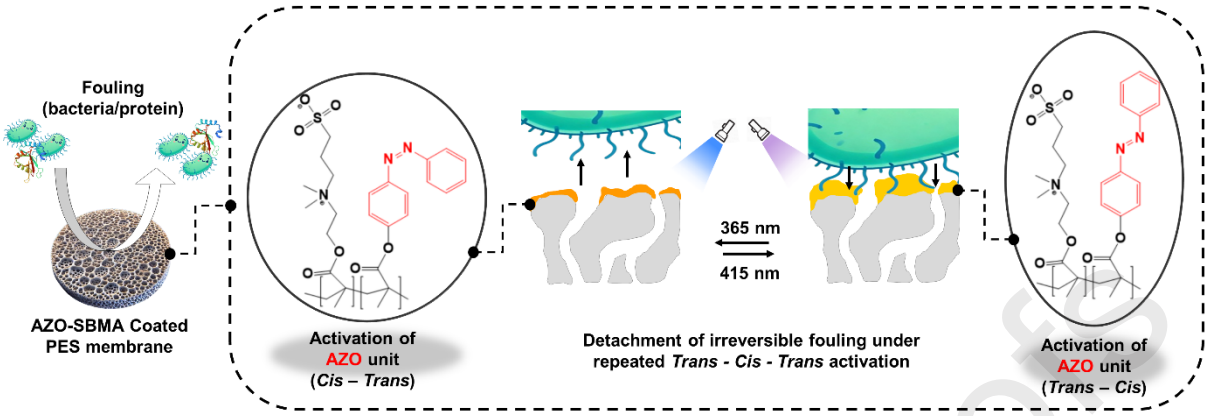

Graphical Abstract

1. Introduction

Membrane-based technology has emerged as an important approach in wastewater treatment, water purification, beverage industry and among others technologies due to its high efficiency, low energy requirements, simplicity in operation and eco-friendliness[1,2]. However, a major challenge with membrane systems is fouling, where a wide range of solutes and suspended species in complex mixtures adsorb onto the membrane surface and pores. This includes contaminants like proteins and polysaccharides, which interact with the membrane through electrostatic attraction and hydrophobic interactions[1,3]. These substances serve as nutrients for bacteria, leading to biofouling through bacterial adhesion and extracellular matrix production[4]. As a result, it decreases water permeability, deteriorates membrane selectivity and shortens membrane lifespan. Hence it requires frequent backwashing or harsh chemical cleaning, increasing cost of membrane processing and posing significant threat to the environment. Traditional antifouling strategies, such as surface hydrophilization or bactericidal coatings, struggle to fully address biofouling. Once it occurred, they often rely on chemicals that contribute to the rise of antimicrobial-resistant (AMR) bacteria[5–7]. Therefore, the development of effective green strategies for fouling control is among the most desired areas of research in membrane science and technology[1,3].

In recent years, stimuli-responsive materials have shown significant potential for developing sustainable antifouling membranes for cleaning and separation processes[1,3,8–12]. These materials can alter their chemical and physical properties in response to external stimuli such as temperature[13], pH[14], light[15–17], or redox[18]. Among them, light is an especially smart external stimulus because of its excellent adjustment of spatial and temporal reactivity[19–23]. Light-responsive chemical groups such as azobenzenes, diarylethenes, spiropyrans can be physically blended or chemically bound within the membrane bulk structure or immobilized by coating or grafting onto the membrane surfaces[10]. Azobenzene and its derivatives stand out for their ease of synthesis and ability to undergo rapid, reversible changes in both geometry (9.9 Å ⇌ 5.5 Å) and dipole moment (0.5 Debye ⇌ 3.1 Debye) through *trans-cis* photoisomerization under UV/Visible irradiations[3,10,19,22,23]. Azobenzene-based materials have been used in a variety of applications such as photolithography[24], information storage[25], actuators[26], solar energy storage[27] and

photoswitchable porous materials[28,29]. In biological context, it has been used for optical manipulations of biomolecular structure (e.g. photoswitchable antimicrobials)[6,8,30–32], peptides, proteins, and nucleic acids in vitro as well as ion channels and receptors in vivo with high spatiotemporal resolution[33,34]. The photoisomerization could decrease the glassy state (glass transition, *Tg*) of azopolymer, changing the volume of azobenzene-containing materials[23,35]. It was reported that azobenzene-based liquid-crystalline elastomer films could be contracted by about 3% in length after exposure to UV light at 100 mW cm^{-2} for 100 s[3,36]. Utilizing those unique properties, Ramanan et. al.[3] reported self-cleaning membranes for water purification by co-depositing photo-mobile 4,4′-azodianiline and a bio-adhesive polydopamine (PDA) on the surface of ultrafiltration (UF) membranes. Once exposed with UV light, AZO undergoes photoisomerization from *trans*-AZO to *cis*-AZO, decreasing the volume, while the exposure to visible light enables the transition from the *cis* to *trans* configuration, increasing the volume. That results in self-cleaning behavior of the modified membranes through the reversible volume change, which was demonstrated in treating 1 g L^{-1} bovine serum albumin (BSA) solution. Whereas according to other studies, azopolymer could undergo a repeated *trans-cis-trans* photoisomerization[37–39] i.e. directional photo-fluidization[38] (different than photoinduced decrease of *Tg*), which has been used for many attractive applications, including light-powered healing of a wearable electrical conductor, inscription of surface relief gratings and smoothing of surface roughness[40,41]. Kehe et. al.[42] demonstrated this ability to disrupt up to 4-log reduction of several robust gram negative/positive bacterial biofilms by opto-mechanically activating the azopolymer coated surface. Interestingly, Tong et al.[11] have reported a Hagfish-inspired slippery liquid-infused porous surface (SLIPS) coating for marine antifouling applications. This coating was based on the supramolecular interaction between azobenzene (AZO) and *α*-cyclodextrin (*α*-CD). The surface demonstrated efficient self-cleaning, anti-protein, antibacterial, and anti-algae properties, along with a 180-day real marine field antifouling performance, by switching lubrication modes and exhibiting self-healing properties. The primary mechanism likely involves reversible light-induced changes in surface volume and physicochemical properties, creating enough mechanical force on azo-modified surfaces to dislodge adhered bacteria.

Although azobenzene polymer modified membranes could have exhibited detachment to nonspecific protein and bacteria after biofouling formation, but without obviously improving the antifouling properties during the filtration experiments. Therefore, it is essential to introduce another functional component to maintain a tight hydration layer at the interfaces wherever the membrane material is probably in contact with nonspecific protein during filtration[43]. Hence, following the requirements for nonfouling[43], the material has to be hydrophilized in order to strengthen the interactions with water. Moreover, electrical neutrality should be maintained to minimize electrostatic interactions with charged segments of proteins or bacterial cell walls. Several nonfouling membranes have been presented, either based on poly(ethylene glycol) (PEG)[44–46] or on zwitterions[47–51]. The advantage of zwitterionic materials over PEG is their higher stability in complex medium where more water molecules can interact with zwitterionic molecule compare to PEG molecule[52]. As an example, sulfobetaine methacrylate (SBMA), a commercially available zwitterionic monomer has been extensively reported for its high fouling resistance property by maintaining zwitterionic activity[53]. Thus, by combining the dynamic properties of azobenzene (AZO) with the antifouling capabilities of SBMA, we aim to modify membranes with superior resistance to fouling while creating the ability to self-clean under light activation. Ultrafiltration (UF) membranes, which have pore sizes in the 2–100 nm range, are especially suited for such applications due to their ability to efficiently separate proteins, bacteria, and other foulants from water[54]. While various approach has been studied to introduce

antifouling additives onto membrane surfaces such as, in situ polymerization/copolymerization[55], O_2 plasma surface grafting[56]. Surface coating offers a particularly cost-effective and scalable solution [57]. Coating requires minimal additives and can be performed without specialized equipment, making it an ideal method for large-scale membrane modification[58].

Therefore, in the present study, we synthesized a copolymer of AZO and SBMA unit (**Figure 1**). The structure-properties of the copolymer has been systematically evaluated by Mass, ^{1}H and COSY NMR. The change in properties of the copolymer due to photoisomerization has been evaluated by UV-vis spectroscopy and differential scanning calorimetry (DSC). The spectral properties of the copolymer have been fully characterized involving all the photokinetic parameters. The modified membranes have been prepared by coating commercial UF PES membrane with the copolymer and the physicochemical properties e.g., Fourier transform infrared spectroscopy (FTIR), scanning electron microscopy (SEM), contact angle and hydration capacities were analyzed. The water permeability and the antifouling performance of the modified membrane were evaluated by using bovine serum albumin (BSA) suspension. The light induced cleaning efficiency of the fouled membrane has been observed by FTIR chemical mapping. Finally, the membranes were subjected to be fouled by bacteria (*P. aeruginosa*) and the detachment of adhered bacterial and biofilm was monitored by epifluorescent microscopy.

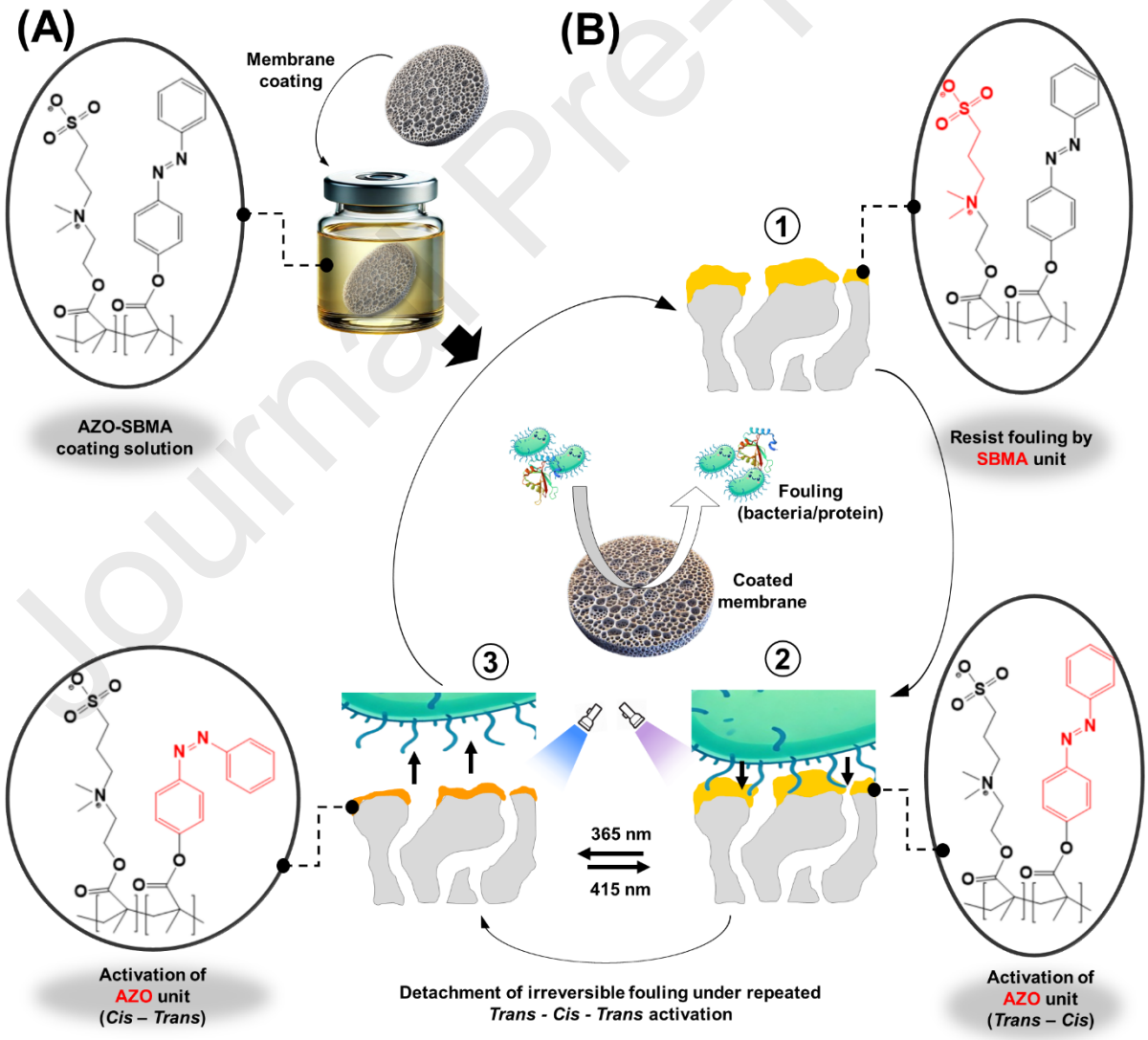

Figure 1. Schematic representation of (A) the dip-coating process of AZO-SBMA on a PES membrane, and (B) the stepwise mechanism of biofouling (bacteria/proteins) detachment. Step 1 (during filtration): SBMA unit resists reversible fouling. Step 2 & 3 (after filtration): AZO unit undergoes *Trans*-*Cis*-*Trans* repeated isomerization under UV-vis light activation to detach irreversible fouling.

2 Experimental Section

2.1 Materials

4-Phenyl azophenol (CAS: 1689-82-3), sulfobetain methacrylate (SBMA) (CAS: 3637-26-1), methacryloyl chloride (CAS: 920-46-7), triethylamine (Et_3N), azobisisobutyronitrile (AIBN) and all the solvents were purchased from Sigma Aldrich. Ultraporous polyethersulfone flat sheet membrane with bulk pore size 0.04 µm was purchased from 3M^{TM} MicroPES. Bovine serum albumin (BSA, 66.5 kDa) and Phosphate buffer saline (PBS) were purchased from Sigma Aldrich. All chemicals and solvents were used directly without further purification as reagent grade. *Pseudomonas aeruginosa* (CIP104116) was purchased from the Institut Pasteur collection (France) as freeze-dried sample. It was cultured in Tryptic Soy Broth (TSB) prior being prepared in PBS 1X for experiments.

2.2 synthesis

2.2.1 Synthesis of 4-Phenyl azophenyl methacrylate (AZO-MA) (3)

4-Phenyl azophenol (**1**) (4.9550 g, 25 mmol), Et_3N (3.7946 g, 37.5 mmol) and 250 ml of dry dichloromethane (DCM) were taken into a 500 ml round bottom flask fitted with an ice-water bath. In the mixture, a solution of methacryloyl chloride (**2**) (3.1359 g, 30 mmol) in dry DCM (100 ml) was added dropwise in stirring condition for 8 h. Then the reaction mixture was stirred overnight at room temperature (**Scheme S1**). After the solvent was removed by rotary evaporation and the residue was washed with 1 M hydrochloric acid, 1 M sodium bicarbonate solution and water sequentially to remove the excess methacryloyl chloride as water soluble methacrylic acid. The organic phase was collected in chloroform ($CHCl_3$) and solvent was evaporated. A yellow product was obtained after the solvent was evaporated. Finally, the solid crude product was dried in vacuum overnight and purified by column chromatography on silica gel with chloroform as eluent. The pure AZO-MA monomer was obtained as a bright orange crystalline product with 90 % yield.

Mass [M+1]: 267.11 [CH_4^+] (**Figure S1**). ^{1}H NMR (400 MHz, $CDCl_3$, δ): 8.00 - 7.92 (m, 4H), 7.53 - 7.50 (m, 3H), 7.31 - 7.29 (m, 2H), 6.40 (m, 1H), 5.80 (m, 1H), 2.10 (dd, 3H) (**Figure S2**). ^{1}H – ^{1}H 2D-COSY NMR spectra was performed (400 MHz) which confirmed Ar-Hs peak via correlation between the neighboring hydrogens (**Figure S3**).

2.2.2. Synthesis and characterization of AZO-SBMA copolymer (5)

Random copolymer of the AZO-SBMA (**5**) was synthesized via typical free radical polymerization in 1:1 molar composition (**Scheme S1**). At first SBMA (**4**) (6.25 g, 22.35 mmol) was taken in DMSO (250 ml) inside a 500 ml round bottomed flask and the solution was warmed (50 °C) in stirring condition for 30 minutes to ensure complete dissolution of the monomer. Then the reaction mixture was cooled down to room temperature. Then AZO-MA (**3**) (5.95 gm, 22.35 mmol) and AIBN (3 mol% of total monomers, 0.22 g, 1.35 mmol) was added and degassed with N_2 gas for 60 minutes. Then the reaction mixture was sealed and the reaction was started at 70 °C for 48 hours. Then the mixture was cooled down to room temperature and exposed to air to stop the reaction. The reaction mixture was slowly poured into a large volume of chilled methanol in stirring condition to precipitate the polymer. Then the precipitate was dried and dissolved in DMSO and re-precipitated twice in order to remove any excess of monomers and impurities. The yellowish orange copolymer was collected, dried in vacuum for 48 hours with 70% yield. The chemical structure of the copolymer was characterized by ^{1}H NMR (400 MHz) in DMSO-d_6 and the characteristic peaks were recognized in **Figure S4**.

2.3 Instruments & characterization

2.3.1 UV-vis absorption spectra

All UV-vis absorption spectra of the AZO-SBMA copolymer in DMSO were recorded on a HP 8452A Diode-Array spectrometer (Olis Global Works software) under dark and controlled temperature (25 °C) with stirring condition using a 10 mm quartz cuvette (**Figure S10**). First, the sample solution 2 ml (18.94×10^{-3} mg ml^{-1}) was taken inside a clean quartz cuvette and the spectrum was recorded without any irradiation. Second, the spectrum was recorded sequentially under two light emitting diodes (LEDs) irradiation at 365 nm (Mightex: WLS-LED-0365-03) to reach the *cis*-PSS and then 415 nm (Mightex: WLS-LED-0415-03) to come back to the *trans*-PSS. The photoisomerizations under irradiation were performed in several cycles to monitor the repeatability. An optic fiber was used to deliver irradiation to the side of sample holder and perpendicularly to the measurement beam. The LEDs were used at their maximal power (110 ± 5 mW cm^{-2}). A stepwise UV-vis photokinetic modeling was conducted (Section **SI 5)** to determine the photochemical properties, such as quantum yields and molar extinction coefficients.

2.3.2 Differential scanning calorimetry (DSC) of the copolymer

Differential scanning calorimetry (DSC Q2000) was measured on the polymer sample before and after irradiation at 365 nm according to the protocol performed elsewhere[23]. DSC

measurements were conducted under a N_2 atmosphere from -50 °C to 150 °C with heating and cooling rates of 10 °C/min. To measure the *trans* form, 10 mg of pure copolymer obtained after polymerization was taken directly. Because it was not possible to convert enough *cis* from *trans* by direct UV irradiation on the polymer powder, the sample was dissolved as suggested in literature[23]. Therefore, 10 mg of the sample was dissolved in 1 ml of Hexafluoroisopropanol (HFiP) solution inside a transparent vial and was irradiated at 365 nm in stirring condition for 90 minutes to generate almost complete conversion to the *cis*-PSS. Despite of the high optical density of concentrated solution, 74% of the *trans* isomer was converted to the *cis* isomer and was checked by UV-vis spectrometer. Then, the vial was connected with a rotary evaporator to remove all the solvent under dark conditions in room temperature (23 °C) for 2 hours. The obtained *cis* isomer was used for DSC experiments.

2.4 Membrane modification & characterization

2.4.1 Surface coating by AZO-SBMA copolymer

Coating of the AZO-SBMA copolymer on the membrane surface was done upon commercial polyethersulfone (PES). The membrane samples were modified by a dip-coating method. The AZO-SBMA copolymer was dissolved in 2,2,2-trifluoroethanol (TFE) inside a 100 ml vial, with concentrations of 1 and 10 mg ml^{-1} prepared for membrane coating. The solution was warmed at 50 °C in stirring condition for 30 minutes to ensure complete dissolution and then cooled down to room temperature. The membrane samples (26 mm diameter) were dipped into the copolymer solution for 5 min. During the first 2 minutes of dipping, sonication was performed to remove any entrapped air from membrane pores and to facilitate homogeneous coating. Then the modified membranes were washed with DI water to detach any loosely adhered copolymer and stored in dark with DI water at 4 °C until use. In the manuscript, the membranes coated with 1 and 10 mg ml^{-1} copolymer concentrations are referred to as AZO-SBMA 1 and AZO-SBMA 10, respectively.

Glass cover slips (1.8 cm × 1.8 cm) was spin coated by SPIN150 spin coater. First, the cover slips were washed with acetone followed by DI water and dried under vacuum. Second, the dried cover slips were fitted inside the spin coater under vacuum and were coated with 150 µl of the copolymer solution at a concentration of 1 mg ml^{-1} for 20 seconds at 1000 rpm. The modified cover slips were collected and stored in the dark and dry condition for further use.

2.4.2 Membrane physico-chemical characterization

Scanning electron microscopy (SEM) analysis (Phenom XL) were done on both modified and unmodified membranes to evaluate the surface and cross sections morphology. Cross-sectional sample was obtained by freeze-fractured method with liquid N_2. All samples were

sputter-coated with gold prior to imaging and analysis were performed at an accelerating voltage of 10 kV. The surface pore size distribution was determined from the SEM images by using ImageJ software[59].

Surface chemistry of the membranes was analyzed by attenuated total reflection (ATR)-Fourier transformed infrared (FTIR) analysis by using a Nexus Nicolet FTIR Spectroscopy system with an ATR diamond crystal at 45° angle. Prior to the examination, 1 cm^2 dried sample was cut and measurements were done on both surfaces (three times) for each sample. Each point was scanned sixteen times with a resolution of 8 cm^{-1} and the spectral range was 400 - 2000 cm^{-1}. The ATR correction was applied before plotting the final spectra.

The coating density was evaluated by gravimetric method, measuring the dry weight of membrane samples before and after surface modification. The difference in weight per unit surface area (mg cm^{-2}) corresponds to the coating density, assuming that the copolymer remained at the surface of the membrane during the coating procedure. 10 measurements were averaged for each sample, leading to the reported value of the coating density.

2.4.3 Membrane wetting and hydration properties

Water contact angle (CA) was determined with an automatic contact angle meter (Kruss DSA 30). Droplets of deionized (DI) water (3 µl volume) were deposited on membrane samples that were fixed on a glass slide using double-sided adhesive tape. Contact angles were measured within 1 to 2 seconds after the droplets were deposited on the membrane prior the complete absorption of the water droplet within 5 to 10 seconds. For each sample, the values reported correspond to the average determined from 10 independent measurements. Contact angle was also performed on coated glass cover slips with an average of 5 independent measurements. The CA was determined using sessile drop method.

Hydration capacity or water uptake of membranes was determined by gravimetric analysis after a 24 h-immersion of the samples in DI water. Knowing the dry weight, wet weight and volume of the membrane sample, amount of water trapped per unit volume (mg cm^{-3}) was evaluated. For each membrane sample, 5 independent tests were performed and the corresponding average was determined.

2.5 Membrane antifouling study

2.5.1 Protein adsorption tests

The adsorption of bovine serum albumin (BSA) protein was studied as model foulant[60,61]. The modified and unmodified membrane samples (26 mm diameter) were placed in 5 ml Eppendorf tubes with 70% ethanol for 0.5 h. Then, ethanol was changed to 1 × PBS (pH 7.4) solution and kept overnight at 4 °C. Then the PBS solution was removed and replaced by 2 ml

of 1 mg ml^{-1} protein solution in 1 × PBS. Incubation of the membrane samples with the protein solution was performed for 2 h at 25 °C in mild shaking conditions. After that, the samples were washed with a known volume of PBS buffer to remove the loosely bounded protein. Then the final concentration of the protein in the total solution was measured by recording the absorbance of solution at 280 nm, using a UV-vis spectrophotometer (Perkin Elmer). Knowing the concentration of protein in the solution and before and after the adsorption step, the amount of protein adhered on the membrane surface (μg cm^{-2}) was evaluated. For each sample three independent experiments were performed.

2.5.2 Flux measurement and BSA fouling study

Pure water permeation study was done on unmodified and modified membranes by using Millipore dead end filtration device (Amicon Stirred Cell Model 8010, 10 ml) with 25 mm diameter of effective surface area. Membrane was fitted inside the device connected to a 5 L water reservoir under N_2 gas pressure. Before measuring the actual water flux, membranes were pre-compacted inside the device under higher pressure (1 bar) using pure water. After reaching a steady state flux, the pressure was reduced to the experimental pressure (0.5 bar). A three-step sequential approach was adopted under the same pressure in one cycle, keeping the same batch of membrane sample and by changing the feed. As a first step, the pure water flux (J_{Wi}) of the membrane was collected for 1 h after stabilization and measured using the following equation:

$$J_{Wi} = [Permeate\ volume\ (L)]/[Area\ (m^2) \times Time\ (h)] \quad (1)$$

As a second step, the protein flux was measured after replacing the pure water inside the reservoir by a BSA protein solution (5 mg ml^{-1}). The BSA permeate flux (J_{BSA}) was collected for 2 hrs. After protein filtration, the membrane was thoroughly cleaned with pure water to remove loosely bounded proteins. Finally, the recovered pure water flux was measured again (J_{Wr}) for 1 h.

From the permeate flux value at the different steps of membrane filtration, the flux recovery ratio (FRR) and the protein fouling (R_t) were calculated using following equations[60,61]:

$$FRR\ \% = \left(\frac{J_{Wr}}{J_{Wi}}\right) \times\ 100 \quad (2)$$

$$R_t = \frac{(J_{Wi} - J_{BSA})}{J_{Wi}} \quad (3)$$

For more in-depth analysis, "Total fouling" due to BSA protein adsorption could be further divided into reversible fouling (R_r) and irreversible fouling (R_{ir}) by using following equation:

$$R_r = \frac{(J_{Wr} - J_{BSA})}{J_{Wi}} \quad (4)$$

$$R_{ir} = \frac{(J_{Wi} - J_{Wr})}{J_{Wi}} \quad (5)$$

2.5.3 Removal of protein from fouled membrane under light irradiation

The light induced cleaning efficiency of the copolymer modified membrane was demonstrated on a membrane sample fouled with BSA after filtration step. Wet membrane sample was taken inside a glass petri dish and submerged in PBS buffer solution. Half of the sample surface was covered by a photomask. The other half was uniformly irradiated at a distance of 3-5 mm from the light source (**Figure S13**). The irradiation with the UV (365 nm) and Vis (415 nm) LEDs with maximum intensity (110 ± 5 mW cm^{-2}) were carried out alternatively and each irradiation was performed for 1 min for 3 cycles. After each UV irradiation, the surface was gently washed with PBS buffer to remove any newly detached protein. Afterwards, the sample was dried in vacuum and 4 mm × 4 mm of the sample was cut by equally considering the covered and irradiated surface area. The sample was then fixed on a glass slide using double-sided tape and FTIR chemical mapping of the membrane was performed to determine the BSA specific peaks at 3310 cm^{-1} using an infrared spectrometer (IN10MX). The measurements were performed with a gold mirror as a reference where external reflection was used as the acquisition mode[59,62]. The chemical mapping was performed in contact mode to collect high intensity peak even for traces of BSA. The IR scanning started from the irradiated surface towards the covered surface to avoid contamination of protein from the unexposed area to the irradiated area. Moreover, the measurement was performed at the lowest pressure to avoid protein detachment by physical forces during analysis. Data were measured on a 50 µm × 50 µm surface for each point (one point was measured every 50 µm) with a spectral resolution of 8 cm^{-1}. Each point was scanned sixteen times and the spectral range is 1000–3800 cm^{-1}. The obtained spectra were not processed further, except for the atmospheric correction.

2.5.4 Antibacterial performance and removal of bacteria under light irradiation

Bacterial fouling study of the modified and unmodified membranes were performed by using gram-negative *Pseudomonas aeruginosa* bacteria. The membranes were taken inside a 12 well plate using polycarbonate inserts (CellCrown, Scaffdex) and kept in 70 % EtOH solution for 0.5 h inside a sterile hood. Then the solution was replaced by 1 × sterile PBS buffer solution for overnight at 4 °C. Then the sample was incubated in bacterial suspension (3.5×10^7 CFU ml^{-1}) for 3 h at 37 °C. After the incubation, the sample was washed gently with sterile PBS to remove unadhered bacteria and taken for light induced bacterial detachment

experiment as described in **Section 2.5.3**. Briefly, half of the wet sample in PBS was covered with a photomask and the other half was exposed alternatively with UV/Vis LED homogeneously. In this case, the UV irradiation was performed for two times and Visible irradiation was performed for one time. After each UV irradiation, the sample was washed gently to remove newly detached bacteria under light activation. Then the sample was fixed with 4% (v/v) glutaraldehyde solution in PBS for 4 hours at 4 °C. Then the membrane was rinsed with PBS solution to remove excess glutaraldehyde. A first set of membranes samples was slowly dehydrated with gradually increasing EtOH fraction and was sputter-coated with Au for SEM imaging. A second set of membrane samples was stained with 10× SYBR™ Green (Invitrogen) and imaged with fluorescence microscopy. For both image analysis, 3 consecutive samples were taken for each membrane and 10 to 50 images were taken for each sample.

3. Result & Discussion

3.1. Structural analysis of the monomer & the random copolymer

The photoresponsive 4-phenyl azophenyl methacrylate (AZO) monomer (3) has been synthesized by slight modification of the previous reports (**Scheme S1**)[63]. In the modified version, excessive washing prior to purification was minimized, leading to an improved yield of the AZO monomer. After purification, mass spectra were analyzed and confirmed the expected product (**Figure S1**). The chemical structure was verified by the ^{1}H NMR study and further analyzed by ^{1}H-^{1}H 2D-COSY NMR (**Figure S2 & S3**). The random copolymers of the photoresponsive AZO and zwitterionic SBMA groups were synthesized using free radical copolymerization following a single-step reaction scheme. The synthesis scheme is robust and, as it could be performed in a single-step, the production of this copolymer will be easily scalable. Unlike the AZO-monomer, the copolymer produced several broad peaks even in the high field ^{1}H NMR spectra (**Figure S4**). This is simply due to the presence of long chain repeat units in the copolymer that create poorer molecular rotation and repeating units being situated in marginally different chemical environments[64]. However, the corresponding chemical shifts due to the presence of AZO-SBMA copolymer have been clearly recognized in the NMR spectra. It was found that the final composition of the copolymer after the polymerization slightly varied compared to the feed ratio (**Figure S4**). Consistent with previous studies, this variation in free radical copolymerization is common and can be attributed to the differing reactivity of the monomers[53].

The pure copolymer was crystalline and yellowish orange in appearance compared to the bright orange AZO monomer (**Figure S2**). The copolymer was found to be insoluble in DI water and most of the organic solvents, making surface modified with this copolymer to be re-washable with common organic solvents for storing purposes. Whereas the copolymer was soluble in DMSO and polar Lewis acidic solvents like Trifluoroethanol (TFE) and Hexafluoroisopropanol (HiFP) (**Table. S1**). It is suggested that zwitterion-containing polymers are sensitive to ionic strength and high polarity of solvents, increasing their solubility[53]. Nevertheless, solubility properties of the copolymer may have contributed positively to make a strong coating on the membrane surface, eliminating any significant leaching or damage later in our experiments.

3.2. Photoreversible isomerization & photokinetic study under UV-vis irradiation

The UV-vis spectra of the polymer solution were measured sequentially without any light irradiation, under UV (365 nm) and finally under Visible light (415 nm) irradiation (**Figure 2A**). Under no light irradiation, the AZO-SBMA copolymer represents the pristine state exclusively in a *trans* (100%) conformation[23,65,66] which was also evidenced by the NMR spectra of the AZO-monomer (**Figure S5**). The absorption maximum of the pristine copolymer solution was near 326 nm, with a weak band near 442 nm due to the π-π* and n-π* transition bands of *trans*-azobenzene[21,23,65,66] respectively. Under UV light irradiation at 365 nm, the intensity of the π-π* transition band at 326 nm decreases and the n-π* transition band at 442 nm increases by reaching the *cis*-PSS. The π-π* transition band also shifts from 326 nm to 288 nm and the n-π* transition band shifts from 442 nm to 436 nm. Under visible light irradiation at 415 nm, the spectrum of the AZO-SBMA recovers to the *trans*-PSS. Although it is worth mentioning that under the UV-vis irradiation, the polymer always reaches the photo stationary state (PSS)[21,23,65,66]. In PSS the polymer is a mixture of *trans* and *cis* where one isomer highly dominates the other. In our case, the *trans-cis and cis-trans* PSS was reached at least 6 times under sequential UV-vis irradiation with no change of intensity (**Figure 2B**), exhibiting robust and facile photoisomerization without any degradation[19,21,23,66]. Recently, Vasantha *et al*.[67] has reported copolymers of zwitterionic styrene-dimethylamine terminated sulfobetaine and azobenzene units connected via maleic anhydride linker and did preliminary photoswitching investigation under UV-vis spectroscopy. It is interesting to notice that, despite few similarities in chemical structure, the normalized UV-vis spectra in their study were quite different. Particularly, in our case the isosbestic point exhibits much better separation between the π-π* and n-π* transition, resulting in a higher quantitative conversion yield compare to their compound.

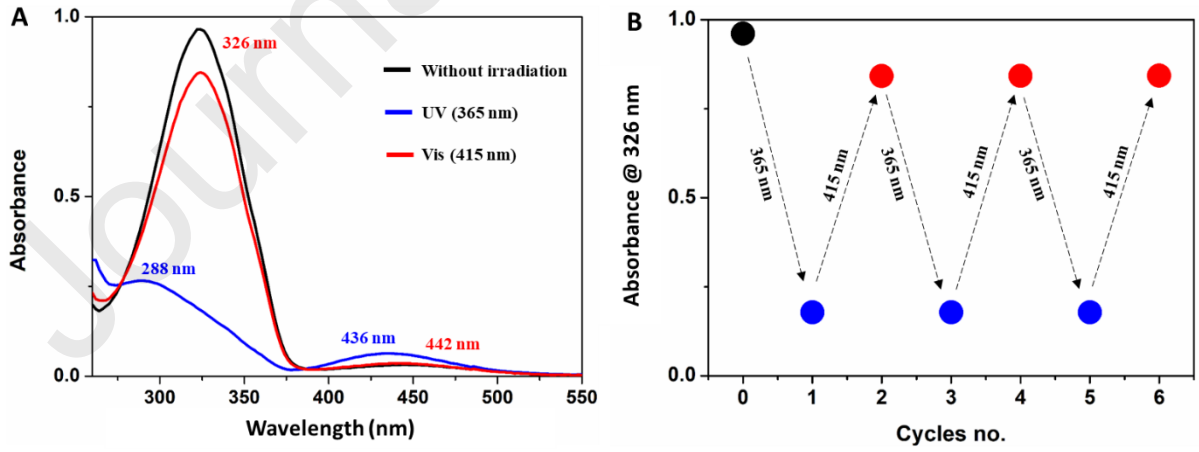

Figure 2. A) Photoisomerization of AZO-SBMA copolymer (5) in DMSO at 25 °C under UV (365 nm) and Visible (415 nm) irradiation. B) Multiple cycles of consecutive photoswitching of the copolymer under UV⇌Vis irradiation. Black: without irradiation (100% Trans), Blue: *Cis*-PSS, Red: *Trans*-PSS.

To assess the photoconversion efficiency of the new AZO-SBMA copolymer, a detailed photokinetic modeling analysis was conducted (**Section SI 5**) to quantitatively determine key parameters such as quantum yields and the molar extinction coefficient (**Table 1**). As shown in **Table 1**, AZOt and AZOc represents *trans→cis and cis→trans* isomerization of azobenzene in both monomer and copolymer. Additionally, Φ_{AZOt}^{366}, Φ_{AZOt}^{416} represents *trans→cis* isomerization quantum yield while Φ_{AZOc}^{366}, Φ_{AZOc}^{416} represents *cis→trans* isomerization quantum yield observed at 366 nm and 416 nm respectively. The same notation applies to the molar extinction coefficient. The observed wavelengths were 1 nm higher than the experimental wavelengths as the UV machine scanned in even numbers.

Table 1. Molar extinction coefficient, quantum yield obtained at the two wavelengths and calculated PSS for the *cis* and *trans* form of the monomer and copolymer

	Molar extinction coefficient (L.mol^{-1}.cm^{-1})				Quantum yield				PSS %	
	ε_{AZOt}^{366}	ε_{AZOt}^{416}	ε_{AZOc}^{366}	ε_{AZOc}^{416}	Φ_{AZOt}^{366}	Φ_{AZOt}^{416}	Φ_{AZOc}^{366}	Φ_{AZOc}^{416}	$[AZOt]$ (1st run)	$[AZOc]$ (2nd run)
AZO-monomer	4650 ± 100	536± 50	160± 50	1200 ± 100	0.15	0.22	0.45	0.48	90	84
AZO-SBMA copolymer	-	-	-	-	0.10	0.15	0.6	0.5	83	88

The quantitative reproduction of the experimental data confirmed that the model was sufficient to account for the observed kinetics. In agreement with the literatures, the *trans→cis* isomerization quantum yield (Φ_{AZOt}^{366}, Φ_{AZOt}^{416}) was found lower than the *cis→trans* isomerization quantum yield (Φ_{AZOc}^{366}, Φ_{AZOc}^{416}) for both monomer and the polymer.

Bandara et. al[68] have reported photoisomerization in different classes of azobenzene. They have found the n→π* excitation corresponds to an isomerization quantum yield Φ_{AZOt}^{416} (*trans→cis*) increase while Φ_{AZOc}^{416} (*cis→trans*) decreases with increasing solvent polarity. Whereas solvent polarity did not change photoisomerization quantum yields (Φ_{AZOt}^{366}, Φ_{AZOc}^{366}) significantly following π → π* excitation. Interestingly, in our case, despite using the same solvent for both AZO-monomer and copolymer, a similar trend in the quantum yield was observed for n→π* excitation. This difference can likely be attributed due to the absence of a zwitterionic group and the lower viscosity of the monomer compared to the polymer. Moreover, the model allowed the precise concentration quantification of the *trans* and *cis* isomers in PSS (**Table 1**) during the photoconversion. In case of the monomer, AZOt reached 90% under 365 nm, AZOc reached 84% under 415 nm. Whereas in copolymer, AZOt reached 83% under 365 nm, AZOc reached 88% under 415 nm. Consistent with our report, recent

works on azo-based switches[69,70] have shown high photoconversion (approx. 90%) with quantum yield Φ^{λ}_{AZOt} of 0.05–0.21. Notably, Zhang et al.[71] has introduced pyrazolylazophenyl ethers (a structural modification of the conventional azobenzene) as a class of azo-photoswitche material that provides excellent performance with near-quantitative (95-98%) *trans→cis→trans* photoisomerization (quantum yield Φ^{λ}_{AZOt} of 0.40−0.44). Therefore, in future, the success of azobenzene-based switches should focus in their structural modification to obtain near-complete photoconversion in both directions.

3.3. Photoinduced solid to quasi-solid transition

The solid to quasi-solid (semi-solid) transition of the AZO-SBMA copolymer under UV irradiation was evaluated measuring glass transition temperature (*Tg*) by differential scanning calorimetry (DSC) (**Figure 3A**) as the standard method[23]. The copolymer was a rather complex system as approximately half of it was consisting of a non-photoresponsive unit. Before any irradiation, the AZO unit was in 100% *trans* and the composition of the copolymer was consisting of 54% AZO and 46% SBMA unit (analyzed in **Figure S4**). Whereas after UV irradiation in the DSC sample, 74% *trans*-AZO was converted to *cis*-AZO (*cis*-AZO PSS is 83%). The percentage of conversion of the copolymer after UV irradiation was verified by UV-vis spectra of the sample (**Figure 3B**). Therefore, after UV irradiation, the final composition consisted of 40% *cis*-AZO, 14 % *trans*-AZO and 46% SBMA (in PSS it should be approximately 45% *cis*-AZO, 9% *trans*-AZO and 46% SBMA). Nevertheless, the DSC thermogram of the copolymer revealed intriguing results. It not only shows the glass transition temperature (*Tg*) before and after irradiation but also highlights the inherent properties of the individual polymers. Usually, the *Tg* appears in both amorphous and semi-crystalline polymers. *Tg* of a polymer corresponds to the temperature above which its molecular chains begin to move, and the polymer undergoes from a glassy solid state to rubbery quasi-solid or plastic state[72]. It is believed that *Tg* of a polymer is greatly influenced by *cis* and *trans* configurations because of the change in free volume, crystallinity, chain stiffness and interchain cohesion of polymer chains[23,35]. It is well recognized that *cis* and *trans* azopolymers could present different *Tg* values[23]. In our case, the glass transition (*Tg*) and melting behavior of the copolymer were not clearly distinguishable before or after UV irradiation, likely due to the overlap of multiple chemical components. However, the direct observation (**Figure 3B, inset**) of the samples suggest that the sample was crystalline and yellowish orange in appearance before irradiation. In contrast, after the UV irradiation, the sample was found quasi-solid and bright red in appearance and most likely with lower *Tg* than the *trans* copolymer. For a better understanding of our DSC thermogram, a detailed analysis of each polymer is necessary.

Firstly, for dry poly-SBMA, no thermal transition should be observed during the heating experiments from −25 to 60 °C, which means the polymer chains should not have any contribution to the endothermic behavior[52,73]. However, the zwitterionic SBMA unit is highly hygroscopic and bound with water molecules so tightly that no thermal transition could be detected either during heating until the ratio of Water : SBMA is larger than 6:1. Up to this ratio, the water and SBMA form a complex, with the water being referred to as "nonfreezable water"[52,73]. This nonfreezable water results from strong electrostatic interactions between the water molecules and the SBMA chains, specifically between the positively charged ($N^{+}(CH_3)_3$) group and the negatively charged (SO_3^{-}) group[52]. Consistent with the literature,

in our case a mild thermal transition close to 0 °C was observed due to the presence of freezable water[52,73]. Freezable water appears when all binding sites of the SBMA are almost completely saturated by water molecules, leading to a thermal transition similar to the ice-to-water phase change seen in bulk water[52,73]. This indicates that, despite drying the sample before the experiment, at least 6 to 8 water molecules remained strongly bound to each SBMA unit in the copolymer. In addition, a strong and broad endothermic peak could be observed at 60 to 100 °C most likely due to the dehydration, or loss of water which was strongly bounded in the polymers[74]. However, due to the presence of photoresponsive AZO polymer unit in the copolymer, the peak seems to appear at a lower temperature than that of poly-SBMA[74]. Numerous investigations have suggested that the strong hydration layer on zwitterionic chains are highly responsible for the antifouling properties of the modified materials that resist non-specific protein adsorption and bacterial cell adhesion[50,58]. Whereas, polyethylene glycol (PEG) modified surface, which has been largely studied, can bind only one water molecule per PEG-unit via hydrogen bonding. In comparison, zwitterionic SBMA can bind an average of 7.86 water molecules per unit with higher degrees of freedom, resulting in superior resistance to non-specific proteins[52,75].

In case of azobenzene unit, it was the only component responsible for decreasing *Tg* of the *trans* copolymer under UV irradiation through an athermal process[23,39], and its effect became more evident in the graph. In *trans* conformation, pure azopolymer usually show glassy, liquid crystalline behavior with *Tg* in the range of 48 to 67 °C[23,35]. The photoinduced *trans* to *cis* conversion could lower the *Tg* well below room temperature, resulting a complete solid-to-liquid phase change[23,35]. However, in our case, the copolymer reaches a quasi-solid state instead of liquid state probably due to the presence of SBMA unit. Moreover, SBMA unit could also create strong intramolecular and intermolecular charge attractions[74], resulting in probable reduction of 'flow' through mass migration in overall copolymer even under UV irradiation. In addition, after UV irradiation, 74% of the *trans*-copolymer is converted to *cis*-copolymer, whereas a conversion of more than 90% of the azopolymer alone was obtained in recent literature[23]. It is believed that increasing *cis* content in the azopolymer has a direct relationship of decreasing *Tg*, where *cis* isomer acts like a plasticizer[23]. The solid to rubbery quasi-solid state acquired by the photoconversion may be just appropriate for our application during membrane cleaning (discussed later). Additionally, the broad endothermic peak of the copolymer decreased from 81°C to 67°C after UV irradiation, and the peak became broader, likely due to more water molecules binding with the cis copolymer. This is due to the fact that the conversion from *trans* to *cis* copolymer creates a significant change in geometry in the overall polymer[3] and generates more amorphous regions available for binding water molecules[23,74]. Furthermore, unlike the *trans*-copolymer, the cis-copolymer showed a liquid crystal (LC) phase transition at 96°C and a broad exothermic band at 110-140°C, due to cis-to-trans thermal isomerization, as previously reported[23].

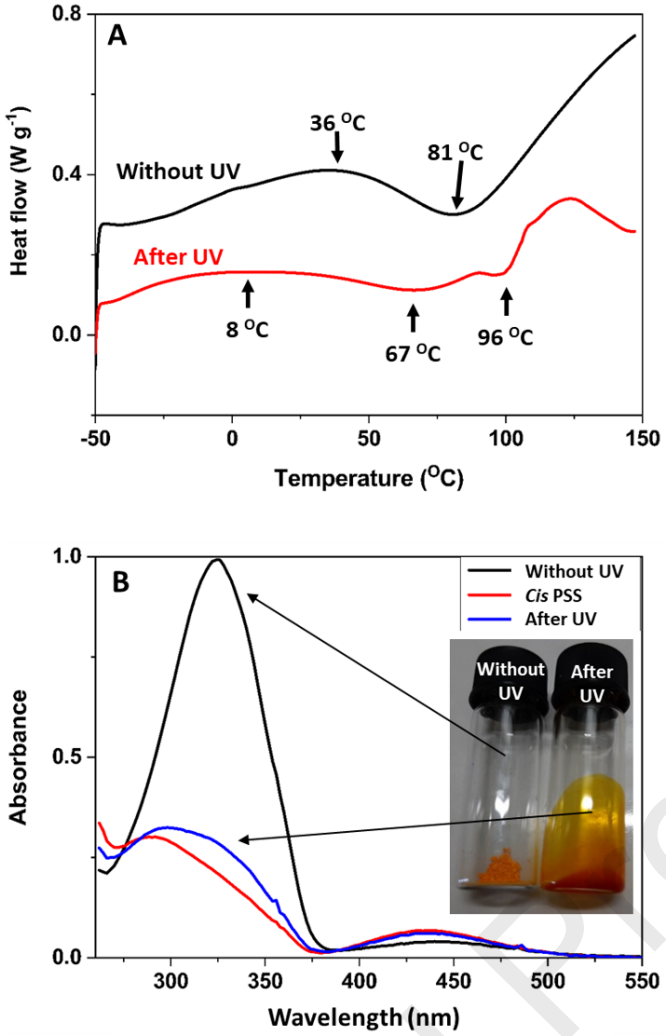

Figure 3. DSC thermogram of the copolymer. A) DSC curve without and after UV irradiation. B) UV-vis spectra of the DSC sample in solvent compare to *cis*-PSS showing that more than 74% of the sample was converted to *cis* after UV (*cis-PSS* 83%). Inset. photographs of the sample taken without and after UV irradiation.

3.4. Understanding the photoinduced conversion mechanism of AZO-SBMA copolymer in relation to conventional azopolymer

The photoinduced solid to quasi-solid transition observed in our study differs from the previous photoinduced solid to liquid transition reported in literature[23], as explained in **Section 3.3** (although both were governed by the same principle). It also differs from the conventional directional "photo-fluidization" seen in azopolymers, such as the formation of surface relief gratings[76]. Generally, directional photo-fluidization is based on photoinduced *trans–cis–trans* cycling, i.e., photoinduced repeated *trans* to *cis* and *cis to trans* isomerization[37,38,77]. Although the detailed mechanism of photo-fluidization of azopolymers is still under study[23,38], such difference could be due to the change of the local environment of the Azo moiety upon photoisomerization corresponding to an increase of the effective temperature[78]. Azopolymers with push–pull group such as pseudo-stilbene

type (e.g., Disperse Red 1) is well suited for *trans–cis–trans* cycling. This is because the absorption bands of *trans* and *cis* isomers overlap, allowing both *trans* to *cis* and *cis to trans* isomerization to be triggered by visible light of the same wavelength. However, the fluid-like state is only maintained when the azopolymer is continuously exposed to polarized light. Moreover, in these type of azobenzene, the direction of the flow is parallel to direction of incident polarized light[23,35,37,38].

In contrast to directional photo-fluidization, the solid to quasi-solid transition reported here arises from the distinct glass transition temperatures (*Tg*) of the *trans* and *cis* copolymers. Specifically, the *trans* copolymer exhibits a glassy-solid state, while the *cis* copolymer adopts a quasi-solid state. More specifically, once the *trans* copolymer is converted to the *cis* copolymer, it remains in the quasi-solid state even when the UV light is turned off. The quasi-solid *cis* copolymer could be returned to the previous solid *trans* copolymer by irradiation in the visible range[23,35]. That means, UV irradiation will mostly produce *trans* to *cis* isomer and visible irradiation will mostly produce *cis* to *trans* isomer in the copolymer. And it could not be interchangeable due to the presence of a well-separated isosbestic point between the π-π* and n-π* transition in the azobenzene unit. In addition, azobenzene unit in the quasi-solid *cis* copolymers are isotropic and the photoinduced reduction of glassy state (*Tg*) is non-directional[23] i.e. independent of polarized light and could be achieved by LEDs. *Cis* copolymers with a long thermal lifetime (**Figure S8**) and high *cis* content like in this study are better suited for photoinduced solid to quasi-solid transitions. Whereas azopolymers with push–pull azobenzene groups have a very short thermal lifetime and are not suitable for photoinduced solid to quasi-solid transitions. An extended UV irradiation was applied on glass slides coated with AZO-SBMA copolymer, and the solid to quasi-solid transition are detailed in **Section S6**.

3.5 Membrane surface chemistry, morphology and physico-chemical characterization

The membrane surface chemistry after coating with two different concentrations of AZO-SBMA copolymer (1 and 10 mg ml^{-1}) was analyzed by ATR-FTIR methods (**Figure 4**). As observed in the IR spectra, the variations of absorption peaks were mainly centered in the region of 1800−1000 cm^{-1}. First, the characteristic peaks of unmodified PES membranes (i.e., 1579, 1486, 1320, 1292, 1244, 1152, and 1107 cm^{-1}) exhibited high absorption intensities[79]. Two typical peaks at 1579 and 1486 cm^{-1} are attributed to aromatic (Ar) ring groups. Peaks located at 1320/1292 and 1152/1107 cm^{-1} are related to the asymmetric and symmetric stretching vibrations of sulfone groups (Ar-SO_2-Ar), respectively. Moreover, a strong peak at 1244 cm^{-1} is due to the presence of aromatic ether structures (Ar-O-Ar). The additional characteristic peaks after coating of copolymer on the modified membrane was clearly detected and is denoted as (*) in the **Figure 4**. The peak located at 1041 cm^{-1} was due to S=O symmetric stretching, confirming the presence of SBMA unit[80]. Whereas two small peaks at 1597 and 1442 cm^{-1} were attributed to N=N stretching[81], confirming the presence of AZO unit on the modified membranes. Additionally, the O−C=O stretching peak at 1744 cm^{-1} was contributed by both the AZO and SBMA unit[9,82–84]. Moreover, the relative intensity of the above characteristic peaks on the modified membranes increased with the coating concentration, which denotes a corresponding increase of copolymer on the modified surface quantitatively. A band at 1667 cm^{-1} on the unmodified PES was also observed due to

the presence of preservative on the 'as received' sample[85]. This band disappeared on the modified samples due to the washing step before coating.

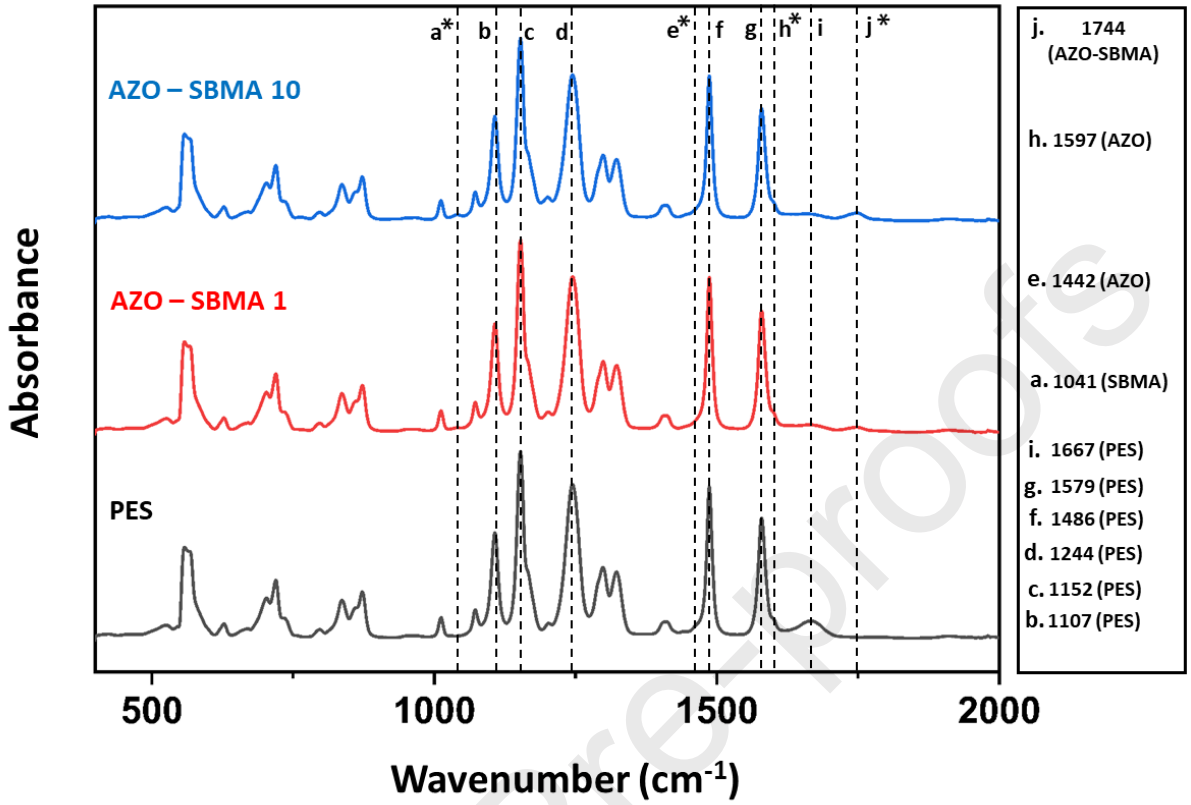

Figure 4. ATR-FTIR spectra of the PES membrane after AZO-SBMA copolymer coating where: unmodified PES in Black, AZO-SBMA 1 in Red and AZO-SBMA 10 in Blue respectively. (*) represents the new peaks after copolymer coating.

Membrane structure morphologies after coating with different concentration of the copolymer were observed by SEM (**Figure 5**). For comparison, real-time digital photographs of the pristine and modified membranes have been taken (**Figure 5AB,C**) which showed a darkening of the yellowish coating on the modified surface by increasing the coating concentration. In general, no significant differences in surface structure could be observed by SEM, when comparing the coated membranes to the pristine membrane. This finding suggests that mostly the surface chemistry has been altered by the coating process, without any major physical changes, which is highly desirable for UF membrane applications. However, small aggregates of copolymers seem to block some of the surface pores on the AZO-SBMA 10 membrane (pointed by white arrows). Therefore, coating assay at higher concentration has not been performed.

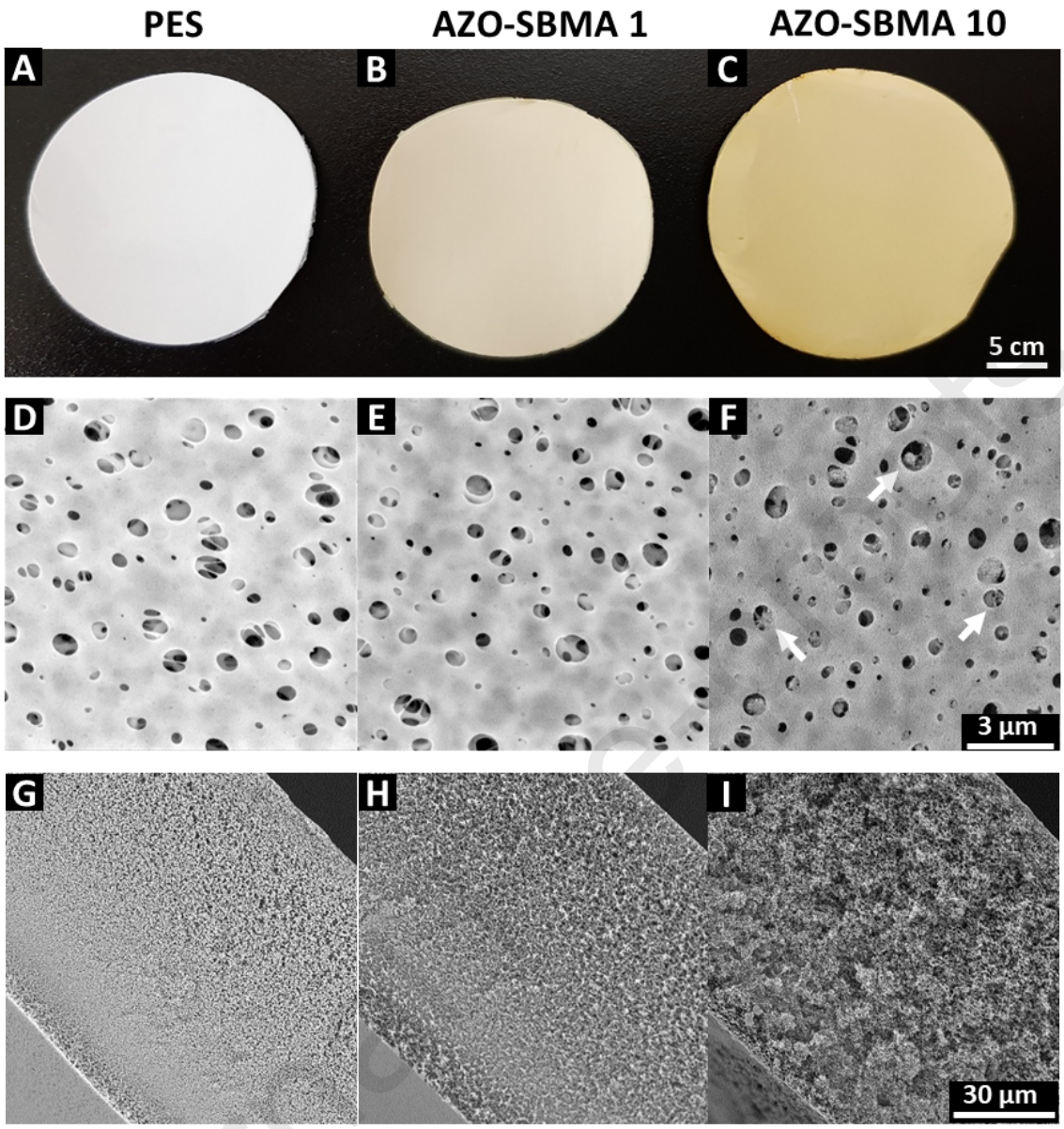

Figure 5. Images of PES membranes before & after dip coating by AZO-SBMA copolymer;

(A-C) Digital photographs, SEM images of (D-F) Surface & (G-I) cross sectional morphology respectively.

Nevertheless, it would be interesting to discuss the coating density and stability of the copolymer in this study as it is consisting of one hydrophilic zwitterionic unit and another relatively hydrophobic azobenzene unit. Coating density and coating stability usually rely on the balance between two opposite forces[58,80]: i) polar forces between the hydrophilic units of the copolymer and the coating solvent environment in which the membranes are likely to be used and ii) hydrophobic forces between the anchoring units of the copolymer and the hydrophobic PES membrane on the other hand. It is believed that the former interactions likely destabilize the system, that could have resulted in lower coating densities[58]. Whereas later interactions are more suitable for stabilizing the coating via hydrophobic-hydrophobic anchoring, resulting in overall increase of coating density with the copolymer concentration

(**Figure 6A**). Particularly, the coating density was increased from 0.11 to 0.31 mg cm^{-2} by increasing the copolymer concentration in the coating solution, from 1 to 10 mg ml^{-1}, suggesting that the hydrophobic interactions may have dominated, leading to stronger bonding between the copolymer and PES. The surface pore size distribution was evaluated from the SEM images by using ImageJ application (**Figure 6B**). The effect of increasing coating concentration did not really have a significant change of porosity, keeping a large number of pores open which is desired after the coating and any membrane modification steps. However, it seems pores size distribution has shifted towards smaller range as the coating density increased, suggesting that the coating blocked some of the larger pores (as evident by the SEM images).

The wetting properties of the membranes were investigated using DI water in air where the contact angle was found 51°, 78° and 84° for pristine PES, AZO-SBMA 1 and AZO-SBMA 10 respectively (**Figure 6C**). These results also indicate that the copolymer was efficiently coated on the PES by increasing the coating concentrations. Usually, the water contact angle of the UF membrane is related to surface chemical modification and as well as surface morphology (roughness, porosity and pore size distribution)[81]. Regardless of increasing polar zwitterionic units, the contact angle of the modified membranes was increasing with coating concentration. It could be due to the increase of the roughness on the porous surface[81]. It is well known that, irrespective of chemical hydrophilicity, contact angle could increase due to reduction of the solid-liquid interfacial contact in the case of micro and nanostructured rough surfaces[86,87]. Moreover, according to previous report, the zwitterionic chains could collapse in air by resisting instantaneous wetting by water[58]. Therefore, the materials could have reduced interaction with foulant in air (e.g., dust particle). However, once immersed in water, the results of hydration capacity (**Figure 6D**) indicates that zwitterionic units get exposed with the surrounding aqueous environment. This allows a greater amount of water to penetrate the membrane material through strong electrostatic attraction, which is crucial for biofouling resistance in membrane processes[58,88]. In addition, the azobenzene unit could exhibit moderate to low contact angles, maintaining sufficient overall hydrophilicity of the modified surface[3,9,11]. Moreover, to understand the surface wetting behavior solely by the chemical modification with minimal contribution from surface roughness, water contact angle was measured on a spin coated glass cover slips (**Figure S11A**). It was found that the spin coated cover slips (coating density 0.77 mg cm^{-2}) has a contact angle of 47° compare to the blank cover slips of 53°, concluding the hydrophilic nature of the copolymer. Results suggests that these properties are characteristic of ideal antifouling surfaces, which exhibit good hydration capacity with the ability to trap water once immersed in aqueous medium, due to expansion of zwitterionic chains[58]. However, AZO-SBMA 10 displayed slightly lower hydration capacity than AZO-SBMA 1, most likely because some of the pores in AZO-SBMA 10 were blocked due to higher coating concentration. Additionally, the unmodified PES membrane, despite its hydrophobic nature, displayed a lower contact angle and higher hydration capacity compared to lab-made PES membranes [81,89–91]. This is likely due to the presence of a hydrophilic layer on the surface, which is commonly applied by commercial suppliers for storage purposes [92]. During the AZO-SBMA coating process in this study, this hydrophilic layer may have been removed, contributing to the observed increase in contact angle after coating.

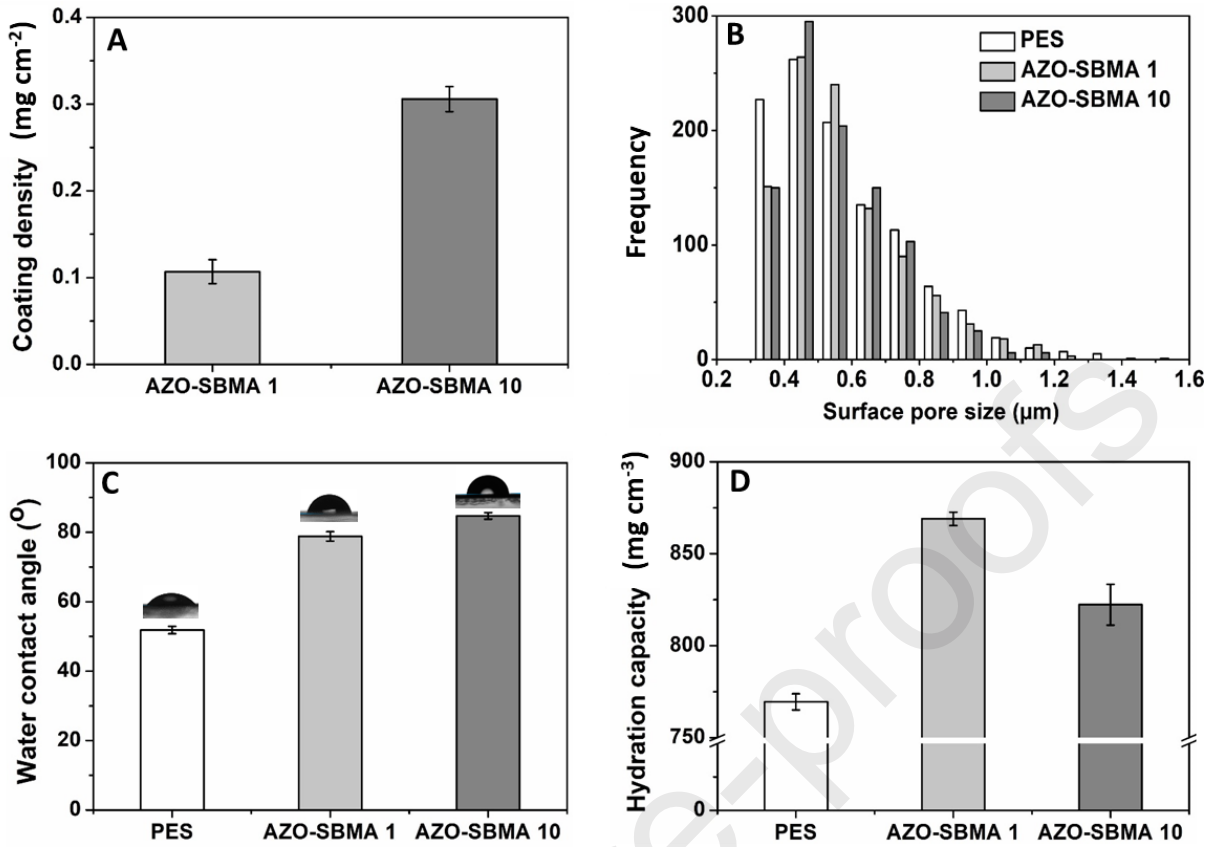

Figure 6. Change in membrane physical and wetting properties after coating of 1 mg ml^{-1} (AZO-SBMA 1) and 10 mg ml^{-1} (AZO-SBMA 10) copolymer; (A) coating density on membrane surface, (B) surface pore size distribution (counted on 53 μm × 53 μm area by ImageJ on SEM images), (C) water contact angle and (D) hydration capacity.

3.6. Membrane antifouling efficiency

3.6.1. Protein adsorption study

Non-specific protein adsorption should be avoided as it directly causes membrane fouling and promotes biofouling by bacteria or proteins in complex wet environments. Hence, resistance to protein adsorption is an important assessment to develop fouling-resistant membranes[50,60]. Here, **Figure 7** depicts the protein adsorption on the membranes under mild shaking conditions after being incubated in 1 mg ml^{-1} BSA solutions. It was found that the modified membrane displayed significant reduction of protein adsorption compared to unmodified PES. And the protein adsorption was gradually decreased by increasing the copolymer concentration. For instance, protein adsorption reduced from 35.42 μg cm^{-2} (100% adsorption) to 14.20 μg cm^{-2} (─ 60% adsorption) and 9.21 μg cm^{-2} (─ 74% adsorption) for unmodified PES, AZO-SBMA 1 and AZO-SBMA 10 respectively. A high degree of protein adsorption on unmodified PES membrane is well known, which is primarily based on its hydrophobic nature. Generally, the interaction between a hydrophobic surface and proteins is strong enough to overcome the internal secondary interaction like disulfide and hydrogen

bonding, resulting in significant adsorption via structural rearrangement of the proteins[60,61]. Whereas zwitterionic unit like SBMA was very well researched as an outstanding antifouling material for resisting non-specific proteins and bacterial cells adhesion[53]. Like hydration capacity, the antifouling efficiency of the modified membrane were most likely dominated by the presence of zwitterionic unit in the copolymer. Specifically, due to the presence of zwitterionic unit in the modified membrane, a tight hydration layer via strong electrostatic attraction under water could readily generate which is highly unfavorable for protein adsorption. In addition, as understood from the previous section, the presence of azobenzene could generate sufficient hydrophilicity on the modified surface which may have contributed positively to resist protein adsorption.

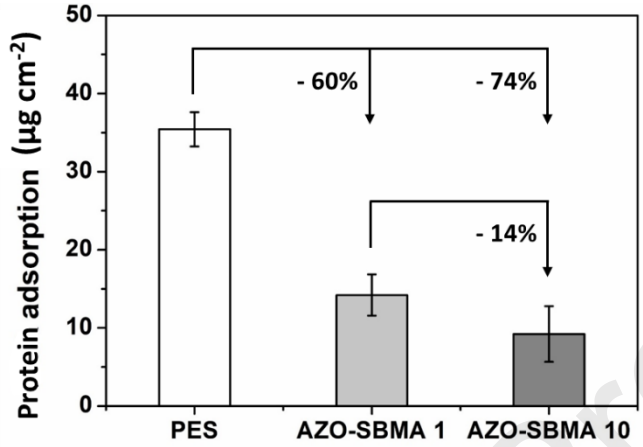

Figure 7. Bovine serum albumin (BSA) protein adsorption on different membranes in PBS buffer (pH 7.4).

3.6.2. Membrane resistance for protein fouling under dynamic filtration study

UF membrane fouling properties directly impact water treatment efficiency, membrane lifespan, and production costs. While protein adsorption tests showed that the AZO-SBMA copolymer resists biofouling, these tests were done under mild shaking conditions. In actual filtration, foulants are pushed through the membrane and interact with the polymer matrix. Thus, dynamic filtration tests provide a more accurate measure of the membrane's antifouling performance[50,60]. Here, in order to understand the dynamic fouling phenomenon, time dependent flux experiments (**Figure 8A**) were performed under transmembrane pressure 0.5 bar that was divided into three steps: pure water permeation (0 to 60 mins), BSA solution (5mg ml^{-1}) filtration (60 to 180 mins) and pure water permeation (180 to 240 mins). Dynamic filtration using BSA as a model foulant is crucial for understanding the membrane's antifouling behavior and the efficiency of removing adsorbed protein through simple washing steps. This process helps identify the nature of the fouling, whether it is reversible or irreversible[50,60]. As depicted in the **Figure 8A**, the decrease in initial pure water flux (J_{Wi}) can be correlated with the increase of copolymer coating concentration via reduction in pores size or blockage of the pores. In addition, after surface modification, an extra resistance towards liquid flow could be expected due to the formation of an additional layer over the pristine PES surface and pores[60,61]. As expected, a dramatic decrease of permanence was

observed with BSA solution (J_{BSA}) for all membranes due to the pore-plugging phenomenon by the BSA protein, resulting from the protein adsorption. However, the washing step was introduced after BSA filtration and the final pure water flux (J_{Wf}) was found to be increased in the modified membranes compared to the pristine PES. This is most likely due to the enhanced hydrophilicity and the formation of a tight hydration layer provided by the zwitterionic copolymer, as demonstrated in previous sections.

Based on these three experimental fluxes, the flux recovery ratio (FRR%) was calculated according **Equation 2** and presented in **Figure 8B**. In comparison to the pristine PES membrane (FRR 39%), a significant increase could be observed on the modified membranes by increasing the coating density. The value for AZO-SBMA 1 was calculated as 76% FRR whereas AZO-SBMA 10 shows more than 88% FRR. For more understanding of the membrane antifouling efficiency, the protein fouling can be defined as total protein fouling (Rt), which is generally caused by adsorption, deposition, and back diffusion on the membrane surface and into the pores. The Rt can be further sub-divided into two fouling components, i.e., reversible (Rr) and irreversible (R_{ir}) fouling as calculated from **Equation 3,4&5** and presented in **Figure 8C**. The irreversible fouling is due to the stable adsorption of foulant molecules that cannot be easily removed, whereas reversible fouling is not stable, and can be washed with a simple hydraulic cleaning[60,91]. The value of R_t and R_{ir} of the membranes were found to decrease steadily by increasing the coating concentration compare to the unmodified PES. Additionally, the degree of reversible fouling (R_r) of the modified membrane was significantly improved. Moreover, AZO-SBMA 10, with its higher concentration of zwitterionic units compared to AZO-SBMA 1, provides enhanced fouling resistance, outweighing the pore size reduction effect[60]. To monitor the extent of fouling and the change in surface morphology of the membranes, SEM images were recorded at the end of filtration experiment (**Figure S12**). The images show patches of proteins on the unmodified membrane surface caused by irreversible fouling leading to the pore size reduction and blockages. On the other hand, the modified membrane maintained a significant number of open surface pores that were not covered by a BSA fouling layer, providing direct evidence of its antifouling properties.

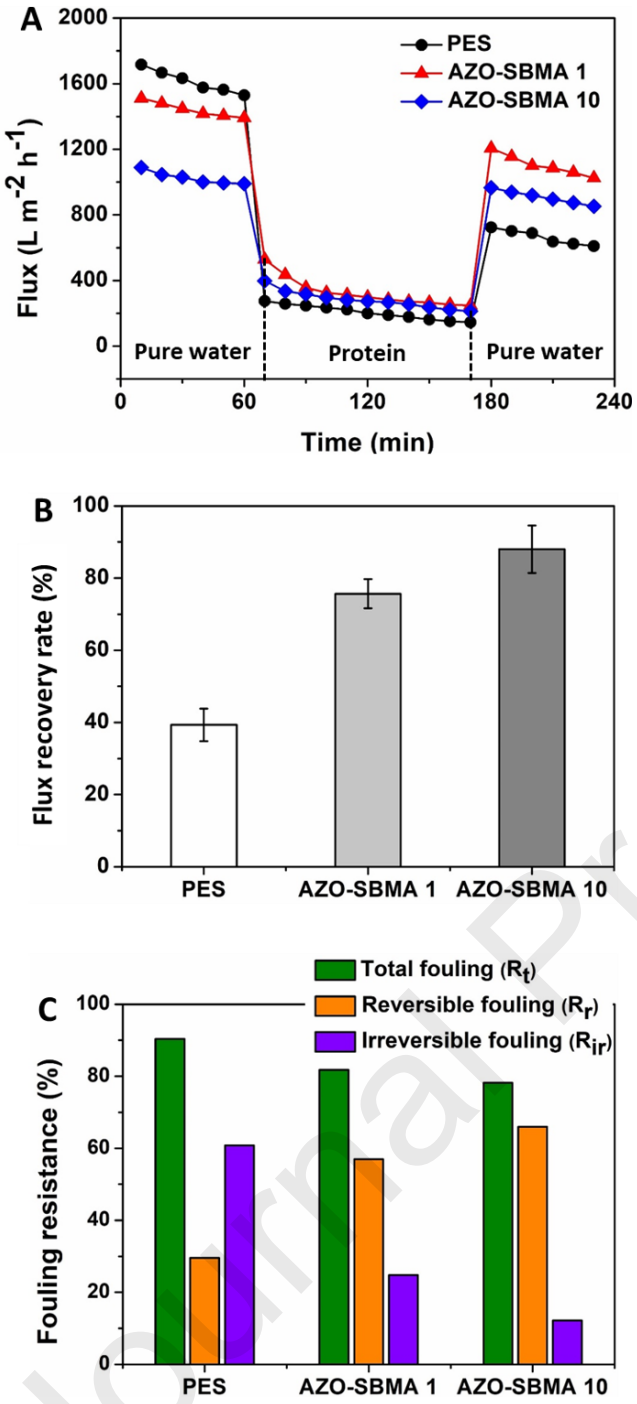

Figure 8. Permeation and antifouling performance of the membranes: A) sequential fluxes with pure water, bovine serum albumin (BSA) protein in PBS solution and the recovered pure water flux after washing step. B) pure water flux recovery rate (FRR%), and C) different types of fouling resistances calculated using resistance-in-series model.

3.7 Light induced anti-fouling and antibacterial performance

3.7.1. Cleaning efficiency of protein fouled membranes

Fouling is a major challenge in membrane filtration. Current cleaning methods, such as physical abrasion, back-flushing, or using harsh chemicals (e.g., bases, acids, biocides), disrupt industrial production and can damage membranes or release harmful by-products into the environment[10].

In this study, fouled membranes from the dynamic flux experiments were cleaned under UV-vis LED irradiation in wet conditions (**Figure S13**), activating the photo-reversible properties of azobenzene in the copolymer. **Figure 9A, B, C** display the FTIR chemical mapping without and after LED irradiation on each membrane sample that represent the distribution of BSA specific peak at 3310 cm^{-1}. From the FTIR mapping, two consecutive observations could be noticed. Firstly, the region without irradiation reveals the modified membrane's superior resistance to reversible BSA adhesion compared to unmodified PES. This likely results due to the presence of zwitterionic SBMA unit in the copolymer, as discussed previously. However, despite the presence of zwitterionic unit, some proteins could still irreversibly bound to the surface. Finally, applying the LED irradiation cycles, it was possible to eliminate majority of the remaining adsorbed proteins, indicating long-term applicability of this surface against fouling. Ramanan et. al.[3] achieved membrane self-cleaning through the photoisomerization of azobenzene, attributing the phenomenon to a reversible change in surface volume. The elongation, swelling, or mass migration of azobenzene-modified materials under light irradiation, leading to changes in surface volume, is well documented previously[11,23,77,93]. A similar phenomenon might have occurred in our present work (as depicted in **Figure 1B**). In addition, azopolymer could impart a significant reversible change in surface roughness[10] and as well as surface chemical properties e.g. hydrophilicity⇌hydrophobicity under light irradiation[8–10,21,94]. These changes in surface chemistry can reversibly promote or hinder protein detachment, likely contributing to the removal of fouling in this study[95–98]. Interestingly, Pouliquen et. al.[99] have reported a reversible binding/de-binding of BSA protein with azobenzene-modified polyacrylate terpolymer under UV-vis irradiation. Under UV exposure, they have achieved up to 80% of BSA release from the BSA/polymer complex which they have thoroughly examined in terms of visco-elastic properties, polymer chain dynamics and binding affinity. Moreover, the presence of non-photoresponsive zwitterionic unit helped resist complete mass migration in the copolymer (discussed in previous **Section 3.4**). A complete mass migration on the membrane sample may have resulted in irreversible changes[93], leading to gradual reduction of repeatability after each photoirradiation cycle. Pirani et. al.[93] have reported a blend of azopolymers with a non-photoresponsive polymer resin for reversible pattering of micro pillars. They showed that the non-photoresponsive polymer's symmetry-breaking properties allowed the micropillars to undergo controlled elongation and rotation under irradiation, with reversible mass migration. No significant structural degradation was observed over multiple cycles. Additionally, SEM images of the membrane sample before and after irradiation were recorded (**Figure S14**), but they provided limited information due to low sensitivity.

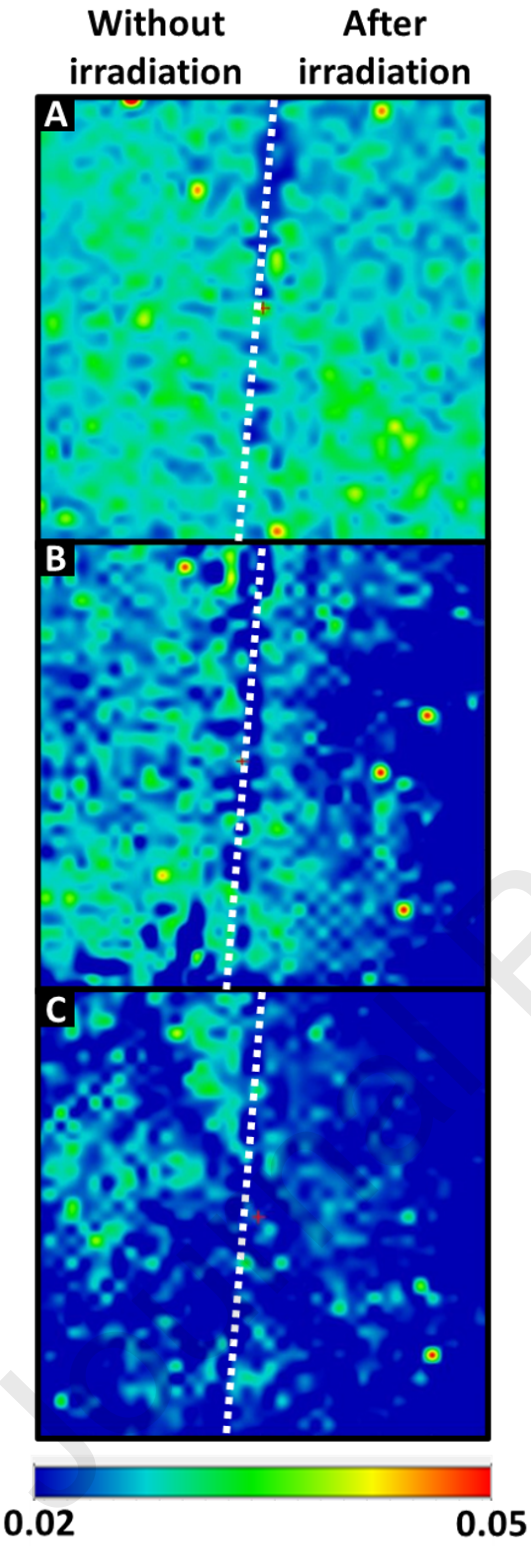

Figure 9. FTIR chemical mapping of bovine serum albumin (BSA) specific peak on A) PES, B) AZO-SBMA 1, C) AZO-SBMA 10 membranes without/after light induced removal of BSA proteins on fouled membranes following sequential flux experiment.

3.7.2. Cleaning efficiency of bacteria fouled membrane

Over recent decades, evolving strategies to combat bacterial growth have been challenged by increasing microbial resistance to both traditional and newer antibiotics[6,100–102]. Antimicrobial resistant (AMR) bacteria such as *Pseudomonas aeruginosa* is most responsible for serious illnesses and prolonged hospital admissions, increasing healthcare costs and water-treatment failures globally[10,42,58,103,104]. The fact that infectious diseases can no longer be treated with antibiotics depicts an unknown future in health care. Hence there is a growing need to examine non-traditional antibiotic strategies that do not rely solely on a targeted biochemical mechanism[6,8,42]. Therefore, in this study, we have attempted a smart approach to remove the bacterial fouling by utilizing the unique photoinduced properties of azobenzene without damaging the bacteria. *Pseudomonas aeruginosa* bacterial biofilms were grown on the unmodified membrane as well as AZO-SBMA copolymer modified membranes. **Figure 10** depicts the SEM images of the bacteria fouled membranes without and after photo irradiation. Similar to protein removal in the above section, here we could notice two consecutive observations. The region without irradiation suggests a significant reduction in bacterial adhesion on modified membrane surfaces compare to unmodified membranes. This demonstrates the effect of SBMA alone to reduce bacterial adhesion as referred in previous studies[58]. On unmodified membranes, numerous bacterial colonies with strong biofilm formation were observed. In contrast, after LED irradiation, modified surfaces showed further bacterial detachment, while the unmodified surfaces retained intact bacterial fouling and normal morphology. This suggests that photoirradiation did not harm the bacteria directly, and their detachment was likely due to a mechanism similar to the protein removal process (as explained in **Section 3.7.1**). Moreover, the light-induced physicochemical changes generated enough mechanical force on the azopolymer-modified surfaces to remove adhered bacteria. This force likely exceeded both the cohesive strength of the biofilm and its adhesion to the surface[11,30,42,105–107]. Lindhorst et al.[30,106] created light-controllable carbohydrate ligands on Au surfaces by integrating *α-d*-mannosyl residues into azobenzene units, which specifically adhere to type 1-fimbriated *E. coli*. The reversible photoisomerization of azobenzene allowed controlled adhesion by changing the ligand orientation without affecting recognition. In the *trans* configuration, azobenzene ligands bind to the fimbrial protein FimH, facilitating bacterial adhesion. Interestingly, UV light at 365 nm induced a conformational change, reducing attached bacteria by fivefold, demonstrating the impact of azobenzene's mechanical reorientation on bacterial detachment.

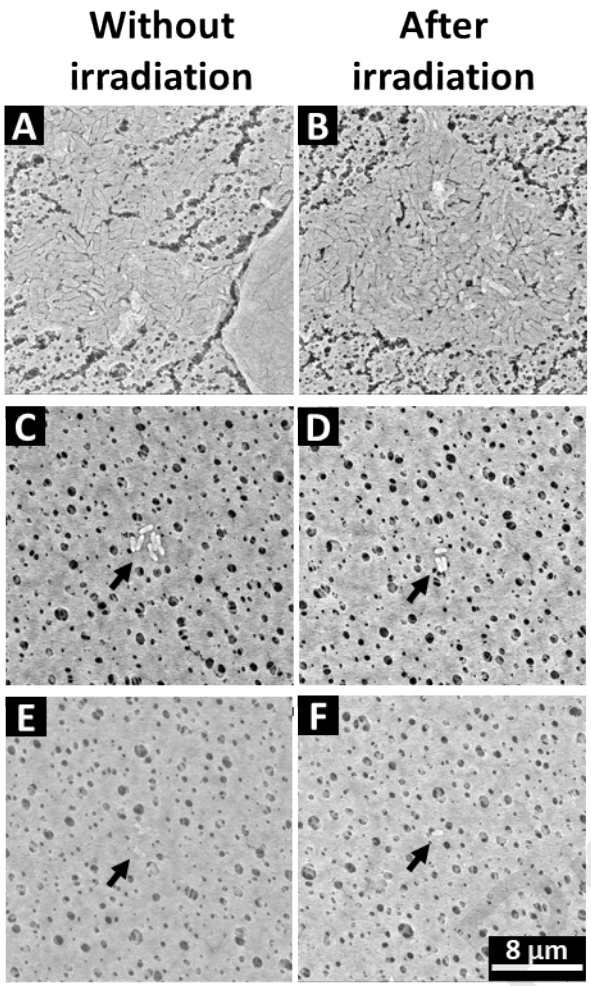

Figure 10. SEM images of different membranes without/after light induced bacterial (*P. aeruginosa*) removal experiments: (A, B) PES, (C, D) AZO-SBMA 1 and (E, F) AZO-SBMA 10, respectively.

To understand the total surface coverage of bacteria on the membrane samples, fluorescence microscopic images were taken on the membrane sample without and after LED irradiation (**Figure S15 & S16**). As evident in the SEM images (**Figure 10**), the fluorescence microscopic images also suggest a very low coverage of bacteria on the modified surfaces compared to pristine PES without any irradiation. In addition, the surface fouling layer was significantly reduced on modified membranes subjected to photoirradiation, indicating the effectiveness of this strategy for membrane surface cleaning. Moreover, on the Pristine PES, several cake layer of bacterial colonies could be observed due to strong biofilm formation. Whereas on the modified membrane, the bacteria were unable to generate such colonies which is the primary step before the biofouling formation. Precisely, unmodified PES has shown the surface coverage of 0.83% and 0.81% without and after LED irradiation respectively. By contrast, AZO-SBMA 1 have shown the surface coverage of 0.45% and 0.073% and AZO-SBMA 10 have shown surface coverage of 0.21% and 0.009% without and after irradiation respectively. The surface of AZO-SBMA 10 detached most bacteria after one irradiation cycle (UV-vis-UV) and, consequently, no irradiation experiments of more than one cycle were carried out, allowing this type of surface to be reusable for long-term applications.

Due to the auto-fluorescence of the pristine PES[108], these images were not as clear as the modified membranes. Therefore, the calculation of surface coverage on the Pristine PES may have underestimated slightly.

Table 2. Comparative analysis with existing light-induced anti-fouling studies.

Study	Antifouling Strategy	Self-cleaning by		Advantages	Disadvantages	[Ref]
		Anti-fouling unit	Light induced unit			
1.	4,4′-azodianiline & polydopamine co-deposited on UF membrane for protein fouling	Yes	Yes	~ 160% increase of water permeance on fouled membrane.	No bacteria fouling studies.	[3]
2.	Acrylated – Azo drop casted on substrate for bacteria fouling	No	Yes	4-log reductions in bacterial biofilms. Non-bactericidal. 5 different bacteria tested. Non-bactericidal.	No protein fouling & filtration studies.	[42]
3.	Azo/CD coating on slippery porous surface for pollutants, proteins, bacteria, algae, and Pseudobarnacle fouling	No	Yes	91.73% self-healing performance. 180-day real marine field antifouling performance. Non-bactericidal.	No filtration studies.	[11]
4.	Azo-ligand coated on Au-substrate for adhesion/removal bacteria	No	Yes	5-fold decrease of adherent bacteria. Non-bactericidal.	No protein fouling & filtration studies.	[106]
5.	Zwitterionic azo polymer for protein fouling & tumor imaging	Yes	Yes	3.1% protein absorption under standard assay.	Non-reversible due to azo-bond breakage. No bacteria fouling & filtration studies.	[109]

6.	Host-guest complexation of zwitterionic azo nanoparticle for protein fouling	Yes	Yes	High stability in blood serum concentration. Nanoparticles aggregation at narrow pH range.	Complicated fabrication. No bacteria fouling & filtration studies.	[110]
7.	Host-guest complexation of azo/CD on Ag-nanoparticle for bacterial fouling	Yes	Yes	~ 84.9% reduction of bacteria. Photo/thermo dual control.	~ 93.2% bacteria killing (bactericidal). Complicated fabrication. No protein fouling & filtration studies.	[111]
8.	Host-guest complexation of azo/CD on substrate for bacteria fouling	No	Yes	~ 4-fold reduction of bacteria under visible green light.	Partly bactericidal. No protein fouling & filtration studies.	[8]
9.	Azo based diaminopyrimidines for in situ control of bacteria	No	Yes	8-fold activity under visible red light (therapeutic window). Non-bactericidal.	Inefficient photoconversion in red light. No protein fouling & filtration studies.	[5]
This work	Zwitterionic azo polymer coated on UF membrane for protein and bacteria fouling	Yes	Yes	~ 88% FRR during filtration & almost removal of fouling after filtration. Non-bactericidal. Photo-kinetic modelling of polymer.	Light induced cleaning not completely under visible light.	-

The development of smart switchable surfaces to address the persistent issue of bacterial attachment and colonization has garnered significant interest. However, achieving on-demand regeneration for non-contaminated surfaces remains a challenge. **Table. 2** provides a comparative analysis of existing light-induced antifouling studies aimed at controlling protein and bacterial fouling. While few studies have explored the combination of light-responsive AZO-based chains and zwitterionic molecules to tackle these issues[67,109–111]. As shown in **Table 2**, these approaches have demonstrated promising antifouling and antibacterial properties. However, they often rely on complex chemical designs for AZO-polymer preparation, which involve high bactericidal activity[111] or breaking of the azo bond[109]. In contrast, this work presents a simpler approach for developing reusable membrane surfaces by removing fouling in a non-bactericidal way. The light-induced cleaning is pathogen-independent, enabling the removal of various types of bacterial fouling regardless of their chemical nature[42]. Additionally, bacteria are unlikely to develop resistance to this mechanism, making it a promising green alternative to conventional antibiotic strategies.

4 Conclusion & outlook

In summary, we developed a light-responsive ultrafiltration membrane with self-cleaning, antifouling, and antibacterial properties. The membrane was modified using dip coating with a copolymer of azobenzene (AZO) and zwitterionic (SBMA) units. Photochemical studies revealed high photoisomerization yields under UV and visible light, along with reversible solid-to-quasi-solid transitions. The modified membranes showed improved physicochemical properties, enhanced protein resistance, better water permeance, and reduced bacterial adhesion (*P. aeruginosa*) without biofilm formation. Upon photoirradiation, nearly all irreversibly bound proteins and bacteria were removed, allowing the fouled membranes to be reusable. This low-cost, non-bactericidal approach offers a promising industrial solution for precise, contactless membrane cleaning, reducing the need for harsh treatments and addressing the challenge of growing antimicrobial resistance (AMR).

Future research could focus on structural modification of AZO-based polymers to achieve near-quantitative photoisomerization using visible or solar light, making the system even more energy-efficient and practical. Such use of light-induced renewable energy to combat membrane fouling offers a more sustainable, low-energy solution. In addition, targeted activation with red light, which can penetrate deeper into tissues without damaging the surrounding environment, holds potential for expanding the application in therapeutic window, particularly in photo-pharmacology.

CRediT authorship contribution statement

PD: Conceptualization, Methodology (all except bacterial culture), validation, Formal analysis, Investigation, Resources, Data curation, Visualization, Writing - Original Draft, Writing - Review & Editing.

NDB: Methodology (bacterial culture)

SD: Technical support, Chemical ordering

JCR, JFL: Writing - Review & Editing, Supervision

VP: Formal analysis & Investigation (UV-vis Photokinetic parameter), Writing -Review & Editing, Supervision

C Coudret: Supervision (UV-vis Photokinetic parameter)

C Coetsier: Conceptualization, Methodology, Writing - Review & Editing, Supervision, Funding acquisition

Acknowledgements

The authors would like to acknowledge the French National Research Agency (ANR-17-CE04-0001), France for funding the project. The authors also would like to thank Corinne Routaboul (Service commun de spectroscopie infrarouge et Raman, Institut de Chimie de Toulouse, Université Toulouse 3, Paul Sabatier, France) and Charaf E. Merzougui (Laboratoire de Génie Chimique, Université Toulouse 3, Paul Sabatier, France) for their kind help to acquire the FTIR chemical mapping images.

Supplementary data

The following are the Supplementary data to this article:

References

[1] H. Zhang, A.U. Mane, X. Yang, Z. Xia, E.F. Barry, J. Luo, Y. Wan, J.W. Elam, S.B. Darling, Visible-Light-Activated Photocatalytic Films toward Self-Cleaning Membranes, Advanced Functional Materials 30 (2020) 2002847. https://doi.org/10.1002/adfm.202002847.

[2] R.P. Lively, D.S. Sholl, From water to organics in membrane separations, Nature Mater 16 (2017) 276–279. https://doi.org/10.1038/nmat4860.

[3] S.N. Ramanan, N. Shahkaramipour, T. Tran, L. Zhu, S.R. Venna, C.-K. Lim, A. Singh, P.N. Prasad, H. Lin, Self-cleaning membranes for water purification by co-deposition of photo-mobile 4,4′-azodianiline and bio-adhesive polydopamine, Journal of Membrane Science 554 (2018) 164–174. https://doi.org/10.1016/j.memsci.2018.02.068.

[4] C. Berne, C.K. Ellison, A. Ducret, Y.V. Brun, Bacterial adhesion at the single-cell level, Nat Rev Microbiol 16 (2018) 616–627. https://doi.org/10.1038/s41579-018-0057-5.

[5] M. Wegener, M.J. Hansen, A.J.M. Driessen, W. Szymanski, B.L. Feringa, Photocontrol of Antibacterial Activity: Shifting from UV to Red Light Activation, J. Am. Chem. Soc. 139 (2017) 17979–17986. https://doi.org/10.1021/jacs.7b09281.

[6] W.A. Velema, J.P. van der Berg, M.J. Hansen, W. Szymanski, A.J.M. Driessen, B.L. Feringa, Optical control of antibacterial activity, Nature Chem 5 (2013) 924–928. https://doi.org/10.1038/nchem.1750.

[7] S. Chen, J. Xie, S. Weng, W. Meng, J. Zheng, B. Huang, R. Zhan, W. Zhang, J. Tian, A supramolecular photosensitizer for combating multiple antibiotic resistance via photodynamic biofilm dispersion, Chemical Engineering Journal 496 (2024) 153951. https://doi.org/10.1016/j.cej.2024.153951.

[8] Q. Bian, S. Chen, Y. Xing, D. Yuan, L. Lv, G. Wang, Host-guest self-assembly toward reversible visible-light-responsive switching for bacterial adhesion, Acta Biomaterialia 76 (2018) 39–45. https://doi.org/10.1016/j.actbio.2018.06.039.

[9] W. Shi, J. Deng, H. Qin, D. Wang, C. Zhao, Poly(ether sulfone) membranes with photo-responsive permeability, Journal of Membrane Science 455 (2014) 357–367. https://doi.org/10.1016/j.memsci.2014.01.005.

[10] E. Pantuso, G.D. Filpo, F.P. Nicoletta, Light-Responsive Polymer Membranes, Advanced Optical Materials 7 (2019) 1900252. https://doi.org/10.1002/adom.201900252.

[11] Z. Tong, L. Song, S. Chen, J. Hu, Y. Hou, Q. Liu, Y. Ren, X. Zhan, Q. Zhang, Hagfish-inspired Smart SLIPS Marine Antifouling Coating Based on Supramolecular: Lubrication Modes Responsively Switching and Self-healing Properties, Advanced Functional Materials 32 (2022) 2201290. https://doi.org/10.1002/adfm.202201290.

[12] J. Yang, H.-J. Ye, H.-M. Xiang, X. Zhou, P.-Y. Wang, S.-S. Liu, B.-X. Yang, H.-B. Yang, L.-W. Liu, S. Yang, Photo-Stimuli Smart Supramolecular Self-Assembly of Azobenzene/β-Cyclodextrin Inclusion Complex for Controlling Plant Bacterial Diseases, Advanced Functional Materials 33 (2023) 2303206. https://doi.org/10.1002/adfm.202303206.

[13] Z.-Q. Shi, Y.-T. Cai, J. Deng, W.-F. Zhao, C.-S. Zhao, Host–Guest Self-Assembly Toward Reversible Thermoresponsive Switching for Bacteria Killing and Detachment, ACS Appl. Mater. Interfaces 8 (2016) 23523–23532. https://doi.org/10.1021/acsami.6b07397.

[14] Q. Zhang, W.-Z. Wang, J.-J. Yu, D.-H. Qu, H. Tian, Dynamic Self-Assembly Encodes A Tri-stable Au–TiO2 Photocatalyst, Advanced Materials 29 (2017) 1604948. https://doi.org/10.1002/adma.201604948.

[15] M. Kathan, F. Eisenreich, C. Jurissek, A. Dallmann, J. Gurke, S. Hecht, Light-driven molecular trap enables bidirectional manipulation of dynamic covalent systems, Nature Chemistry 10 (2018) 1031–1036. https://doi.org/10.1038/s41557-018-0106-8.

[16] F. Eisenreich, M. Kathan, A. Dallmann, S.P. Ihrig, T. Schwaar, B.M. Schmidt, S. Hecht, A photoswitchable catalyst system for remote-controlled (co)polymerization in situ, Nature Catalysis 1 (2018) 516–522. https://doi.org/10.1038/s41929-018-0091-8.

[17] P.K. Kundu, D. Samanta, R. Leizrowice, B. Margulis, H. Zhao, M. Börner, T. Udayabhaskararao, D. Manna, R. Klajn, Light-controlled self-assembly of non-photoresponsive nanoparticles, Nature Chemistry 7 (2015) 646–652. https://doi.org/10.1038/nchem.2303.

[18] Q. Zhang, Z. Zhang, H. Zhou, Z. Xie, L. Wen, Z. Liu, J. Zhai, X. Diao, Redox switch of ionic transport in conductive polypyrrole-engineered unipolar nanofluidic diodes, Nano Res. 10 (2017) 3715–3725. https://doi.org/10.1007/s12274-017-1585-4.

[19] H. Yan, C. Teh, S. Sreejith, L. Zhu, A. Kwok, W. Fang, X. Ma, K.T. Nguyen, V. Korzh, Y. Zhao, Functional Mesoporous Silica Nanoparticles for Photothermal-Controlled Drug Delivery In Vivo, Angewandte Chemie International Edition 51 (2012) 8373–8377. https://doi.org/10.1002/anie.201203993.

[20] M. Morimoto, M. Irie, A Diarylethene Cocrystal that Converts Light into Mechanical Work, J. Am. Chem. Soc. 132 (2010) 14172–14178. https://doi.org/10.1021/ja105356w.

[21] H.S. Lim, J.T. Han, D. Kwak, M. Jin, K. Cho, Photoreversibly Switchable Superhydrophobic Surface with Erasable and Rewritable Pattern, J. Am. Chem. Soc. 128 (2006) 14458–14459. https://doi.org/10.1021/ja0655901.

[22] M.R. Molla, P. Rangadurai, L. Antony, S. Swaminathan, J.J. de Pablo, S. Thayumanavan, Dynamic actuation of glassy polymersomes through isomerization of a single azobenzene unit at the block copolymer interface, Nature Chemistry 10 (2018) 659–666. https://doi.org/10.1038/s41557-018-0027-6.

[23] H. Zhou, C. Xue, P. Weis, Y. Suzuki, S. Huang, K. Koynov, G.K. Auernhammer, R. Berger, H.-J. Butt, S. Wu, Photoswitching of glass transition temperatures of azobenzene-containing polymers induces reversible solid-to-liquid transitions, Nature Chem 9 (2017) 145–151. https://doi.org/10.1038/nchem.2625.

[24] A. Kravchenko, A. Shevchenko, V. Ovchinnikov, A. Priimagi, M. Kaivola, Optical Interference Lithography Using Azobenzene-Functionalized Polymers for Micro- and Nanopatterning of Silicon, Advanced Materials 23 (2011) 4174–4177. https://doi.org/10.1002/adma.201101888.

[25] S. Wu, S. Duan, Z. Lei, W. Su, Z. Zhang, K. Wang, Q. Zhang, Supramolecular bisazopolymers exhibiting enhanced photoinduced birefringence and enhanced stability of birefringence for four-dimensional optical recording, J. Mater. Chem. 20 (2010) 5202–5209. https://doi.org/10.1039/C000073F.

[26] L. Zhang, H. Liang, J. Jacob, P. Naumov, Photogated humidity-driven motility, Nature Communications 6 (2015) 1–12. https://doi.org/10.1038/ncomms8429.

[27] T.J. Kucharski, N. Ferralis, A.M. Kolpak, J.O. Zheng, D.G. Nocera, J.C. Grossman, Templated assembly of photoswitches significantly increases the energy-storage capacity of solar thermal fuels, Nature Chemistry 6 (2014) 441–447. https://doi.org/10.1038/nchem.1918.

[28] L. Ren, J. Chen, J. Han, J. Liang, H. Wu, Biomimetic construction of smart nanochannels in covalent organic framework membranes for efficient ion separation, Chemical Engineering Journal 482 (2024) 148907. https://doi.org/10.1016/j.cej.2024.148907.

[29] J. Chen, X. Chen, U. Azhar, X. Yang, C. Zhou, M. Yan, H. Li, C. Zong, Flexible and Photo-responsive superwetting surfaces based on porous materials coated with Mussel-Inspired Azo-Copolymer, Chemical Engineering Journal 466 (2023) 143176. https://doi.org/10.1016/j.cej.2023.143176.

[30] G. Despras, L. Möckl, A. Heitmann, I. Stamer, C. Bräuchle, T.K. Lindhorst, A Photoswitchable Trivalent Cluster Mannoside to Probe the Effects of Ligand Orientation in Bacterial Adhesion, ChemBioChem 20 (2019) 2373–2382. https://doi.org/10.1002/cbic.201900269.

[31] M. Chen, B. Qiu, Z. Zhang, S. Xie, Y. Liu, T. Xia, X. Li, Light-triggerable and pH/lipase-responsive release of antibiotics and β-lactamase inhibitors from host-guest self-assembled micelles to combat biofilms and resistant bacteria, Chemical Engineering Journal 424 (2021) 130330. https://doi.org/10.1016/j.cej.2021.130330.

[32] Y. Yang, J. Liu, M. Chen, P. Gao, Y. Gong, R. Chen, Y. Tang, W. Yang, K. Cai, Photolithographic-based stamp technique for improving the biocompatibility of antibacterial titanium implant by dynamic clearance of antibacterial agents, Chemical Engineering Journal 421 (2021) 129756. https://doi.org/10.1016/j.cej.2021.129756.

[33] A.A. Beharry, G.A. Woolley, Azobenzene photoswitches for biomolecules, Chem. Soc. Rev. 40 (2011) 4422–4437. https://doi.org/10.1039/C1CS15023E.

[34] C. Hoppmann, P. Schmieder, P. Domaing, G. Vogelreiter, J. Eichhorst, B. Wiesner, I. Morano, K. Rück-Braun, M. Beyermann, Photocontrol of Contracting Muscle Fibers, Angewandte Chemie International Edition 50 (2011) 7699–7702. https://doi.org/10.1002/anie.201101398.

[35] P. Weis, W. Tian, S. Wu, Photoinduced Liquefaction of Azobenzene-Containing Polymers, Chemistry – A European Journal 24 (2018) 6494–6505. https://doi.org/10.1002/chem.201704162.

[36] M. Kondo, R. Miyasato, Y. Naka, J. Mamiya, M. Kinoshita, Y. Yu, C.J. Barrett, T. Ikeda, Photomechanical properties of azobenzene liquid-crystalline elastomers, Liquid Crystals 36 (2009) 1289–1293. https://doi.org/10.1080/02678290903138711.

[37] P. Karageorgiev, D. Neher, B. Schulz, B. Stiller, U. Pietsch, M. Giersig, L. Brehmer, From anisotropic photo-fluidity towards nanomanipulation in the optical near-field, Nature Materials 4 (2005) 699–703. https://doi.org/10.1038/nmat1459.

[38] S. Lee, H.S. Kang, J.-K. Park, Directional Photofluidization Lithography: Micro/Nanostructural Evolution by Photofluidic Motions of Azobenzene Materials, Advanced Materials 24 (2012) 2069–2103. https://doi.org/10.1002/adma.201104826.

[39] N. Hurduc, B.C. Donose, A. Macovei, C. Paius, C. Ibanescu, D. Scutaru, M. Hamel, N. Branza-Nichita, L. Rocha, Direct observation of athermal photofluidisation in azo-polymer films, Soft Matter 10 (2014) 4640–4647. https://doi.org/10.1039/C4SM00397G.

[40] H.S. Kang, H.-T. Kim, J.-K. Park, S. Lee, Light-Powered Healing of a Wearable Electrical Conductor, Advanced Functional Materials 24 (2014) 7273–7283. https://doi.org/10.1002/adfm.201401666.

[41] S. Lee, H.S. Kang, J.-K. Park, High-Resolution Patterning of Various Large-Area, Highly Ordered Structural Motifs by Directional Photofluidization Lithography: Sub-30-nm Line, Ellipsoid, Rectangle, and Circle Arrays, Advanced Functional Materials 21 (2011) 1770–1778. https://doi.org/10.1002/adfm.201001927.

[42] G.M. Kehe, D.I. Mori, M.J. Schurr, D.P. Nair, Optically Responsive, Smart Anti-Bacterial Coatings via the Photofluidization of Azobenzenes, ACS Appl. Mater. Interfaces 11 (2019) 1760–1765. https://doi.org/10.1021/acsami.8b21058.

[43] E. Ostuni, R.G. Chapman, R.E. Holmlin, S. Takayama, G.M. Whitesides, A Survey of Structure−Property Relationships of Surfaces that Resist the Adsorption of Protein, Langmuir 17 (2001) 5605–5620. https://doi.org/10.1021/la010384m.

[44] F. Gao, G. Zhang, Q. Zhang, X. Zhan, F. Chen, Improved Antifouling Properties of Poly(Ether Sulfone) Membrane by Incorporating the Amphiphilic Comb Copolymer with Mixed Poly(Ethylene Glycol) and Poly(Dimethylsiloxane) Brushes, Ind. Eng. Chem. Res. 54 (2015) 8789–8800. https://doi.org/10.1021/acs.iecr.5b02864.

[45] Y. Liu, Y. Su, X. Zhao, Y. Li, R. Zhang, Z. Jiang, Improved antifouling properties of polyethersulfone membrane by blending the amphiphilic surface modifier with crosslinked hydrophobic segments, Journal of Membrane Science 486 (2015) 195–206. https://doi.org/10.1016/j.memsci.2015.03.045.

[46] W. Ma, S. Rajabzadeh, A.R. Shaikh, Y. Kakihana, Y. Sun, H. Matsuyama, Effect of type of poly(ethylene glycol) (PEG) based amphiphilic copolymer on antifouling properties of copolymer/poly(vinylidene fluoride) (PVDF) blend membranes, Journal of Membrane Science 514 (2016) 429–439. https://doi.org/10.1016/j.memsci.2016.05.021.

[47] P.-F. Ren, Y. Fang, L.-S. Wan, X.-Y. Ye, Z.-K. Xu, Surface modification of polypropylene microfiltration membrane by grafting poly(sulfobetaine methacrylate) and poly(ethylene glycol): Oxidative stability and antifouling capability, Journal of Membrane Science 492 (2015) 249–256. https://doi.org/10.1016/j.memsci.2015.05.029.

[48] Y.-F. Mi, F.-Y. Zhao, Y.-S. Guo, X.-D. Weng, C.-C. Ye, Q.-F. An, Constructing zwitterionic surface of nanofiltration membrane for high flux and antifouling performance, Journal of Membrane Science 541 (2017) 29–38. https://doi.org/10.1016/j.memsci.2017.06.091.

[49] D.M. Davenport, J. Lee, M. Elimelech, Efficacy of antifouling modification of ultrafiltration membranes by grafting zwitterionic polymer brushes, Separation and Purification Technology 189 (2017) 389–398. https://doi.org/10.1016/j.seppur.2017.08.034.

[50] G.V. Dizon, A. Venault, Direct in-situ modification of PVDF membranes with a zwitterionic copolymer to form bi-continuous and fouling resistant membranes, Journal of Membrane Science 550 (2018) 45–58. https://doi.org/10.1016/j.memsci.2017.12.065.

[51] S.-L. Li, X. Shan, Y. Zhao, Y. Hu, Fabrication of a Novel Nanofiltration Membrane with Enhanced Performance via Interfacial Polymerization through the Incorporation of a New Zwitterionic Diamine Monomer, ACS Appl. Mater. Interfaces 11 (2019) 42846–42855. https://doi.org/10.1021/acsami.9b15811.

[52] J. Wu, W. Lin, Z. Wang, S. Chen, Y. Chang, Investigation of the Hydration of Nonfouling Material Poly(sulfobetaine methacrylate) by Low-Field Nuclear Magnetic Resonance, Langmuir 28 (2012) 7436–7441. https://doi.org/10.1021/la300394c.

[53] P. Kaner, E. Rubakh, D.H. Kim, A. Asatekin, Zwitterion-containing polymer additives for fouling resistant ultrafiltration membranes, Journal of Membrane Science 533 (2017) 141–159. https://doi.org/10.1016/j.memsci.2017.03.034.

[54] R.W. Baker, Membrane Technology and Applications, John Wiley & Sons, 2012.

[55] T. Xiang, C.-D. Luo, R. Wang, Z.-Y. Han, S.-D. Sun, C.-S. Zhao, Ionic-strength-sensitive polyethersulfone membrane with improved anti-fouling property modified by zwitterionic polymer via in situ cross-linked polymerization, Journal of Membrane Science 476 (2015) 234–242. https://doi.org/10.1016/j.memsci.2014.11.045.

[56] J. Zhao, Q. Shi, S. Luan, L. Song, H. Yang, H. Shi, J. Jin, X. Li, J. Yin, P. Stagnaro, Improved biocompatibility and antifouling property of polypropylene non-woven fabric membrane by surface grafting zwitterionic polymer, Journal of Membrane Science 369 (janvier 3) 5–12. https://doi.org/10.1016/j.memsci.2010.10.046.

[57] B. Yuan, Q. Chen, W.-Q. Ding, P.-S. Liu, S.-S. Wu, S.-C. Lin, J. Shen, Y. Gai, Copolymer Coatings Consisting of 2-Methacryloyloxyethyl Phosphorylcholine and 3-Methacryloxypropyl Trimethoxysilane via ATRP To Improve Cellulose Biocompatibility, ACS Appl. Mater. Interfaces 4 (2012) 4031–4039. https://doi.org/10.1021/am3008399.

[58] S.-H. Tang, A. Venault, C. Hsieh, G.V. Dizon, C.-T. Lo, Y. Chang, A bio-inert and thermostable zwitterionic copolymer for the surface modification of PVDF membranes, Journal of Membrane Science 598 (2020) 117655. https://doi.org/10.1016/j.memsci.2019.117655.

[59] P. Das, J.-C. Remigy, J.-F. Lahitte, A.D. van der Meer, B. Garmy-Susini, C. Coetsier, S. Desclaux, P. Bacchin, Development of double porous poly (ε -caprolactone)/chitosan polymer as tissue engineering scaffold, Materials Science and Engineering: C 107 (2020) 110257. https://doi.org/10.1016/j.msec.2019.110257.

[60] K. Nayak, A. Kumar, P. Das, B.P. Tripathi, Amphiphilic antifouling membranes by polydopamine mediated molecular grafting for water purification and oil/water separation, Journal of Membrane Science 630 (2021) 119306. https://doi.org/10.1016/j.memsci.2021.119306.

[61] B.P. Tripathi, P. Das, F. Simon, M. Stamm, Ultralow Fouling Membranes by Surface Modification with Functional Polydopamine, European Polymer Journal (n.d.). https://doi.org/10.1016/j.eurpolymj.2017.12.006.

[62] L. Benavente, C. Coetsier, A. Venault, Y. Chang, C. Causserand, P. Bacchin, P. Aimar, FTIR mapping as a simple and powerful approach to study membrane coating and fouling, Journal of Membrane Science 520 (12) 477–489. https://doi.org/10.1016/j.memsci.2016.07.061.

[63] S. Wu, X. Zhu, J. Yang, J. Nie, A facile photopolymerization method for fabrication of pH and light dual reversible stimuli-responsive surfaces, Chem. Commun. 51 (2015) 5649–5651. https://doi.org/10.1039/C4CC10441B.

[64] S. Selvasekarapandian, G. Hirankumar, J. Kawamura, N. Kuwata, T. Hattori, 1H solid state NMR studies on the proton conducting polymer electrolytes, Materials Letters 59 (2005) 2741–2745. https://doi.org/10.1016/j.matlet.2005.04.018.

[65] J. Royes, C. Courtine, C. Lorenzo, N. Lauth-de Viguerie, A.-F. Mingotaud, V. Pimienta, Quantitative Kinetic Modeling in Photoresponsive Supramolecular

Chemistry: The Case of Water-Soluble Azobenzene/Cyclodextrin Complexes, J. Org. Chem. 85 (2020) 6509–6518. https://doi.org/10.1021/acs.joc.0c00461.

[66] A.A. Beharry, O. Sadovski, G.A. Woolley, Azobenzene Photoswitching without Ultraviolet Light, J. Am. Chem. Soc. 133 (2011) 19684–19687. https://doi.org/10.1021/ja209239m.

[67] V.A. Vasantha, C. Junhui, Z. Wenguang, A.M. van Herk, A. Parthiban, Reversible Photo- and Thermoresponsive, Self-Assembling Azobenzene Containing Zwitterionic Polymers, Langmuir 35 (2019) 1465–1474. https://doi.org/10.1021/acs.langmuir.8b01820.

[68] H.M.D. Bandara, S.C. Burdette, Photoisomerization in different classes of azobenzene, Chem. Soc. Rev. 41 (2012) 1809–1825. https://doi.org/10.1039/C1CS15179G.

[69] Z.-Y. Zhang, Y. He, Z. Wang, J. Xu, M. Xie, P. Tao, D. Ji, K. Moth-Poulsen, T. Li, Photochemical Phase Transitions Enable Coharvesting of Photon Energy and Ambient Heat for Energetic Molecular Solar Thermal Batteries That Upgrade Thermal Energy, J. Am. Chem. Soc. 142 (2020) 12256–12264. https://doi.org/10.1021/jacs.0c03748.

[70] A.M. Kolpak, J.C. Grossman, Azobenzene-Functionalized Carbon Nanotubes As High-Energy Density Solar Thermal Fuels, Nano Lett. 11 (2011) 3156–3162. https://doi.org/10.1021/nl201357n.

[71] Z.-Y. Zhang, Y. He, Y. Zhou, C. Yu, L. Han, T. Li, Pyrazolylazophenyl Ether-Based Photoswitches: Facile Synthesis, (Near-)Quantitative Photoconversion, Long Thermal Half-Life, Easy Functionalization, and Versatile Applications in Light-Responsive Systems, Chemistry – A European Journal 25 (2019) 13402–13410. https://doi.org/10.1002/chem.201902897.

[72] Y. Yue, Y. Norikane, R. Azumi, E. Koyama, Light-induced mechanical response in crosslinked liquid-crystalline polymers with photoswitchable glass transition temperatures, Nat Commun 9 (2018) 3234. https://doi.org/10.1038/s41467-018-05744-x.

[73] Y.-Y. Jhan, R.-Y. Tsay, Salt effects on the hydration behavior of zwitterionic poly(sulfobetaine methacrylate) aqueous solutions, Journal of the Taiwan Institute of Chemical Engineers 45 (2014) 3139–3145. https://doi.org/10.1016/j.jtice.2014.08.022.

[74] R. Lalani, L. Liu, Synthesis, characterization, and electrospinning of zwitterionic poly(sulfobetaine methacrylate), Polymer 52 (2011) 5344–5354. https://doi.org/10.1016/j.polymer.2011.09.015.

[75] Q. Shao, Y. He, A.D. White, S. Jiang, Difference in Hydration between Carboxybetaine and Sulfobetaine, J. Phys. Chem. B 114 (2010) 16625–16631. https://doi.org/10.1021/jp107272n.

[76] Md.Z. Alam, T. Ohmachi, T. Ogata, T. Nonaka, S. Kurihara, Photoisomerization behavior and photoinduced surface relief gratings on azopolymer film by a monochromatic light irradiation, Optical Materials 29 (2006) 365–370. https://doi.org/10.1016/j.optmat.2005.10.005.

[77] H.S. Kang, H. Cho, W. Panatdasirisuk, S. Yang, Hierarchical membranes with size-controlled nanopores from photofluidization of electrospun azobenzene polymer fibers, J. Mater. Chem. A 5 (2017) 18762–18769. https://doi.org/10.1039/C7TA05313D.

[78] J. Vapaavuori, A. Laventure, C.G. Bazuin, O. Lebel, C. Pellerin, Submolecular Plasticization Induced by Photons in Azobenzene Materials, J. Am. Chem. Soc. 137 (2015) 13510–13517. https://doi.org/10.1021/jacs.5b06611.

[79] Z. Zhou, G. Huang, Y. Xiong, M. Zhou, S. Zhang, C.Y. Tang, F. Meng, Unveiling the Susceptibility of Functional Groups of Poly(ether sulfone)/Polyvinylpyrrolidone Membranes to NaOCl: A Two-Dimensional Correlation Spectroscopic Study, Environ. Sci. Technol. 51 (2017) 14342–14351. https://doi.org/10.1021/acs.est.7b03952.

[80] C.-C. Lien, L.-C. Yeh, A. Venault, S.-C. Tsai, C.-H. Hsu, G.V. Dizon, Y.-T. Huang, A. Higuchi, Y. Chang, Controlling the zwitterionization degree of alternate copolymers for minimizing biofouling on PVDF membranes, Journal of Membrane Science 565 (2018) 119–130. https://doi.org/10.1016/j.memsci.2018.07.054.

[81] Z. Liu, Z. Mi, S. Jin, C. Wang, D. Wang, X. Zhao, H. Zhou, C. Chen, The influence of sulfonated hyperbranched polyethersulfone-modified halloysite nanotubes on the compatibility and water separation performance of polyethersulfone hybrid ultrafiltration membranes, Journal of Membrane Science 557 (2018) 13–23. https://doi.org/10.1016/j.memsci.2018.04.019.

[82] T. Xiang, L.-R. Wang, L. Ma, Z.-Y. Han, R. Wang, C. Cheng, Y. Xia, H. Qin, C.-S. Zhao, From Commodity Polymers to Functional Polymers, Sci Rep 4 (2014) 4604. https://doi.org/10.1038/srep04604.

[83] R. Zhou, P.-F. Ren, H.-C. Yang, Z.-K. Xu, Fabrication of antifouling membrane surface by poly(sulfobetaine methacrylate)/polydopamine co-deposition, Journal of Membrane Science 466 (2014) 18–25. https://doi.org/10.1016/j.memsci.2014.04.032.

[84] D. Wang, X. Zhang, S. Nie, W. Zhao, Y. Lu, S. Sun, C. Zhao, Photoresponsive Surface Molecularly Imprinted Poly(ether sulfone) Microfibers, Langmuir 28 (2012) 13284–13293. https://doi.org/10.1021/la302687d.

[85] S. Belfer, R. Fainchtain, Y. Purinson, O. Kedem, Surface characterization by FTIR-ATR spectroscopy of polyethersulfone membranes-unmodified, modified and protein fouled, Journal of Membrane Science 172 (2000) 113–124. https://doi.org/10.1016/S0376-7388(00)00316-1.

[86] A. Marmur, The Lotus Effect: Superhydrophobicity and Metastability, Langmuir 20 (2004) 3517–3519. https://doi.org/10.1021/la036369u.

[87] L. Feng, Y. Zhang, J. Xi, Y. Zhu, N. Wang, F. Xia, L. Jiang, Petal Effect: A Superhydrophobic State with High Adhesive Force, Langmuir 24 (2008) 4114–4119. https://doi.org/10.1021/la703821h.

[88] S. Chen, L. Li, C. Zhao, J. Zheng, Surface hydration: Principles and applications toward low-fouling/nonfouling biomaterials, Polymer 51 (2010) 5283–5293. https://doi.org/10.1016/j.polymer.2010.08.022.

[89] L.-J. Zhu, L.-P. Zhu, Y.-F. Zhao, B.-K. Zhu, Y.-Y. Xu, Anti-fouling and anti-bacterial polyethersulfone membranes quaternized from the additive of poly(2-dimethylamino ethyl methacrylate) grafted SiO2 nanoparticles, J. Mater. Chem. A 2 (2014) 15566–15574. https://doi.org/10.1039/C4TA03199G.

[90] N. Nasrollahi, S. Aber, V. Vatanpour, N.M. Mahmoodi, Development of hydrophilic microporous PES ultrafiltration membrane containing CuO nanoparticles with improved antifouling and separation performance, Materials Chemistry and Physics 222 (2019) 338–350. https://doi.org/10.1016/j.matchemphys.2018.10.032.

[91] H. Koulivand, A. Shahbazi, V. Vatanpour, M. Rahmandoust, Development of carbon dot-modified polyethersulfone membranes for enhancement of nanofiltration, permeation and antifouling performance, Separation and Purification Technology 230 (2020) 115895. https://doi.org/10.1016/j.seppur.2019.115895.

[92] Membrana documents, (n.d.). https://www.3m.com/3M/en_US/membrana-us/resources/documents/ (accessed August 6, 2021).

[93] F. Pirani, A. Angelini, F. Frascella, R. Rizzo, S. Ricciardi, E. Descrovi, Light-Driven Reversible Shaping of Individual Azopolymeric Micro-Pillars, Scientific Reports 6 (2016) 31702. https://doi.org/10.1038/srep31702.

[94] Z. Chen, H.-Y. Xie, Y.-J. Li, G.-E. Chen, S.-J. Xu, Z.-L. Xu, Smart light responsive polypropylene membrane switching reversibly between hydrophobicity and hydrophilicity for oily water separation, Journal of Membrane Science 638 (2021) 119704. https://doi.org/10.1016/j.memsci.2021.119704.

[95] F. Zhang, A. Zarrine-Afsar, M.S. Al-Abdul-Wahid, R.S. Prosser, A.R. Davidson, G.A. Woolley, Structure-Based Approach to the Photocontrol of Protein Folding, J. Am. Chem. Soc. 131 (2009) 2283–2289. https://doi.org/10.1021/ja807938v.

[96] J. Zhang, T. Hu, Y. Liu, Y. Ma, J. Dong, L. Xu, Y. Zheng, H. Yang, G. Wang, Photoswitched Protein Adsorption on Electrostatically Self-Assembled Azobenzene Films, ChemPhysChem 13 (2012) 2671–2675. https://doi.org/10.1002/cphc.201200231.

[97] Lee C. Ted, K.A. Smith, T.A. Hatton, Photocontrol of Protein Folding: The Interaction of Photosensitive Surfactants with Bovine Serum Albumin, Biochemistry 44 (2005) 524–536. https://doi.org/10.1021/bi048556c.

[98] S. Kneissl, E.J. Loveridge, C. Williams, M.P. Crump, R.K. Allemann, Photocontrollable Peptide-Based Switches Target the Anti-Apoptotic Protein Bcl-xL, ChemBioChem 9 (2008) 3046–3054. https://doi.org/10.1002/cbic.200800502.

[99] G. Pouliquen, C. Tribet, Light-Triggered Association of Bovine Serum Albumin and Azobenzene-Modified Poly(acrylic acid) in Dilute and Semidilute Solutions, Macromolecules 39 (2006) 373–383. https://doi.org/10.1021/ma0512152.

[100] M. Tyers, G.D. Wright, Drug combinations: a strategy to extend the life of antibiotics in the 21st century, Nature Reviews Microbiology 17 (2019) 141–155. https://doi.org/10.1038/s41579-018-0141-x.

[101] M. Raffatellu, Learning from bacterial competition in the host to develop antimicrobials, Nature Medicine 24 (2018) 1097–1103. https://doi.org/10.1038/s41591-018-0145-0.

[102] S.H. Podolsky, The evolving response to antibiotic resistance (1945–2018), Palgrave Communications 4 (2018) 1–8. https://doi.org/10.1057/s41599-018-0181-x.

[103] P. Dadgostar, Antimicrobial Resistance: Implications and Costs, Infection and Drug Resistance (2019). https://doi.org/10.2147/IDR.S234610.

[104] X. Wang, P. Cheng, N. Liu, Y. Wan, Q. Guo, Q. Cheng, K. Liu, Z. Lu, M. Li, D. Wang, Highly efficient nanofibrous sterile membrane with anti-BSA/RNA-fouling surface via plasma-assisted carboxylation process, Journal of Membrane Science 601 (2020) 117935. https://doi.org/10.1016/j.memsci.2020.117935.

[105] D. Yu, X. Xiao, C. Shokoohi, Y. Wang, L. Sun, Z. Juan, M.J. Kipper, J. Tang, L. Huang, G.S. Han, H.S. Jung, J. Chen, Recent Advances in Stimuli-Responsive Smart Membranes for Nanofiltration, Advanced Functional Materials 33 (2023) 2211983. https://doi.org/10.1002/adfm.202211983.

[106] T. Weber, V. Chandrasekaran, I. Stamer, M.B. Thygesen, A. Terfort, T.K. Lindhorst, Switching of Bacterial Adhesion to a Glycosylated Surface by Reversible Reorientation of the Carbohydrate Ligand, Angewandte Chemie International Edition 53 (2014) 14583–14586. https://doi.org/10.1002/anie.201409808.

[107] S. Aggarwal, R.M. Hozalski, Determination of biofilm mechanical properties from tensile tests performed using a micro-cantilever method, Biofouling 26 (2010) 479–486. https://doi.org/10.1080/08927011003793080.

[108] P. Le-Clech, Y. Marselina, Y. Ye, R.M. Stuetz, V. Chen, Visualisation of polysaccharide fouling on microporous membrane using different characterisation techniques, Journal of Membrane Science 290 (2007) 36–45. https://doi.org/10.1016/j.memsci.2006.12.012.

[109] J. Shen, W. Zhang, Y. He, AIEgen-Terminated Charge-Switchable Zwitterionic Azo Polymer for Tumor Hypoxia Imaging, ACS Appl. Polym. Mater. 4 (2022) 6659–6666. https://doi.org/10.1021/acsapm.2c01011.

[110] C. Stoffelen, J. Huskens, Zwitterionic supramolecular nanoparticles: self-assembly and responsive properties, Nanoscale 7 (2015) 7915–7919. https://doi.org/10.1039/C5NR01526J.

[111] Y. Ni, D. Zhang, Y. Wang, X. He, J. He, H. Wu, J. Yuan, D. Sha, L. Che, J. Tan, J. Yang, Host–Guest Interaction-Mediated Photo/Temperature Dual-Controlled Antibacterial Surfaces, ACS Appl. Mater. Interfaces 13 (2021) 14543–14551. https://doi.org/10.1021/acsami.0c21626.

Figure 1. Schematic representation of (A) the dip-coating process of AZO-SBMA on a PES membrane, and (B) the stepwise mechanism of biofouling (bacteria/proteins) detachment. Step 1 (during filtration): SBMA unit resists reversible fouling. Step 2 & 3 (after filtration):

AZO unit undergoes *Trans-Cis-Trans* repeated isomerization under UV-vis light activation to detach irreversible fouling.

Figure 2. A) Photoisomerization of AZO-SBMA copolymer (5) in DMSO at 25 °C under UV (365 nm) and Visible (415 nm) irradiation. B) Multiple cycles of consecutive photoswitching of the copolymer under UV⇌Vis irradiation. Black: without irradiation (100% Trans), Blue: *Cis*-PSS, Red: *Trans*-PSS.

Figure 3. DSC thermogram of the copolymer. A) DSC curve without and after UV irradiation. B) UV-vis spectra of the DSC sample in solvent compare to *cis*-PSS showing that more than 74% of the sample was converted to *cis* after UV (*cis-PSS* 83%). Inset. photographs of the sample taken without and after UV irradiation.

Figure 4. ATR-FTIR spectra of the PES membrane after AZO-SBMA copolymer coating where: unmodified PES in Black, AZO-SBMA 1 in Red and AZO-SBMA 10 in Blue respectively. (*) represents the new peaks after copolymer coating.

Figure 5. Images of PES membranes before & after dip coating by AZO-SBMA copolymer;

(A-C) Digital photographs, SEM images of (D-F) Surface & (G-I) cross sectional morphology respectively.

Figure 6. Change in membrane physical and wetting properties after coating of 1 mg ml^{-1} (AZO-SBMA 1) and 10 mg ml^{-1} (AZO-SBMA 10) copolymer; (A) coating density on membrane surface, (B) surface pore size distribution (counted on 53 µm × 53 µm area by ImageJ on SEM images), (C) water contact angle and (D) hydration capacity.

Figure 7. Bovine serum albumin (BSA) protein adsorption on different membranes in PBS buffer (pH 7.4).

Figure 8. Permeation and antifouling performance of the membranes: A) sequential fluxes with pure water, bovine serum albumin (BSA) protein in PBS solution and the recovered pure water flux after washing step. B) pure water flux recovery rate (FRR%), and C) different types of fouling resistances calculated using resistance-in-series model.

Figure 9. FTIR chemical mapping of bovine serum albumin (BSA) specific peak on A) PES, B) AZO-SBMA 1, C) AZO-SBMA 10 membranes without/after light induced removal of BSA proteins on fouled membranes following sequential flux experiment.

Figure 10. SEM images of different membranes without/after light induced bacterial (*P. aeruginosa*) removal experiments: (A, B) PES, (C, D) AZO-SBMA 1 and (E, F) AZO-SBMA 10, respectively.

Highlights

- Synthesized light-responsive zwitterionic azobenzene coating for UF membrane.
- Coated membrane shows excellent antifouling with BSA protein during filtration.
- UV-vis photoirradiation of azobenzene units cleaned foulants, restoring permeability.
- Modified membrane resisted bacterial adhesion and efficiently removed bacteria under photoirradiation.
- Such light-responsive self-cleaning materials can mitigate concerns about resistant bacteria.

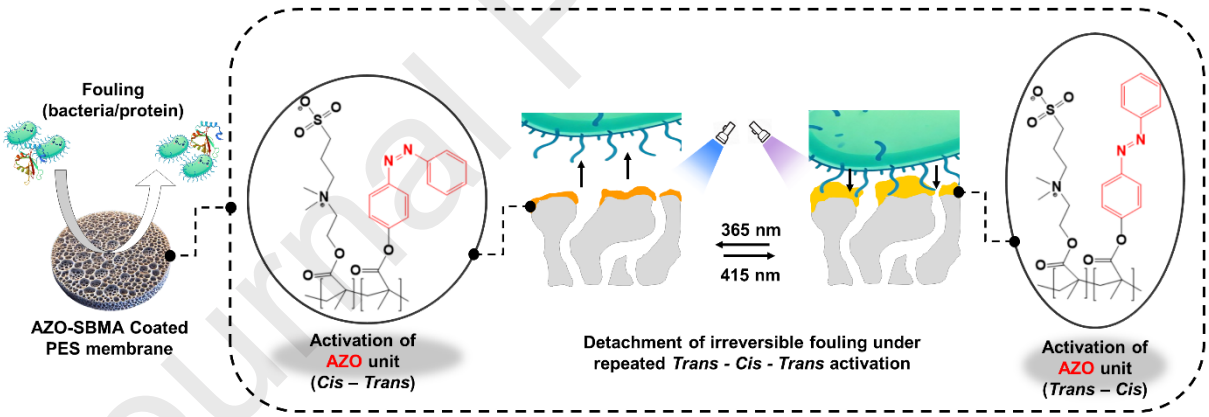

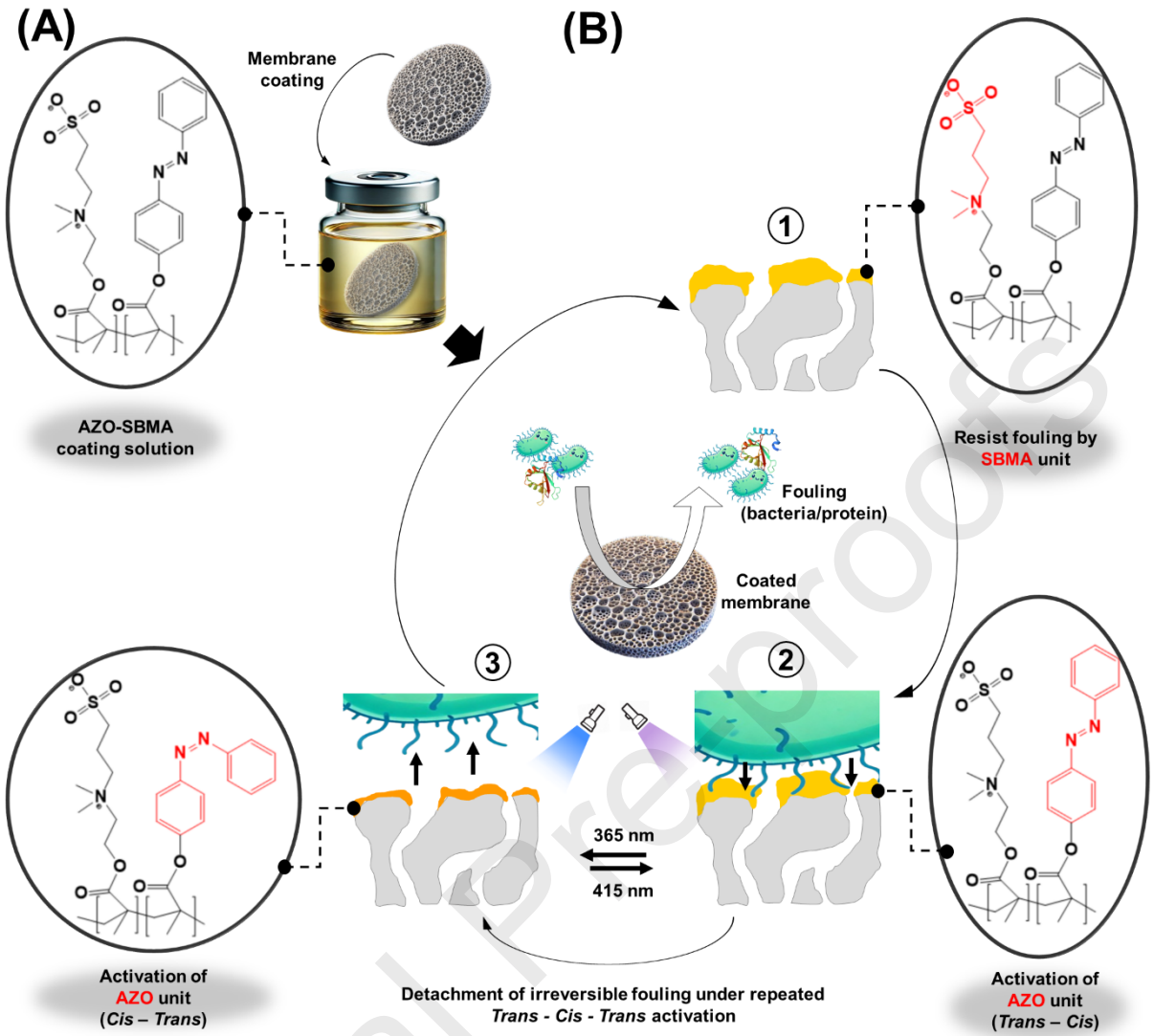

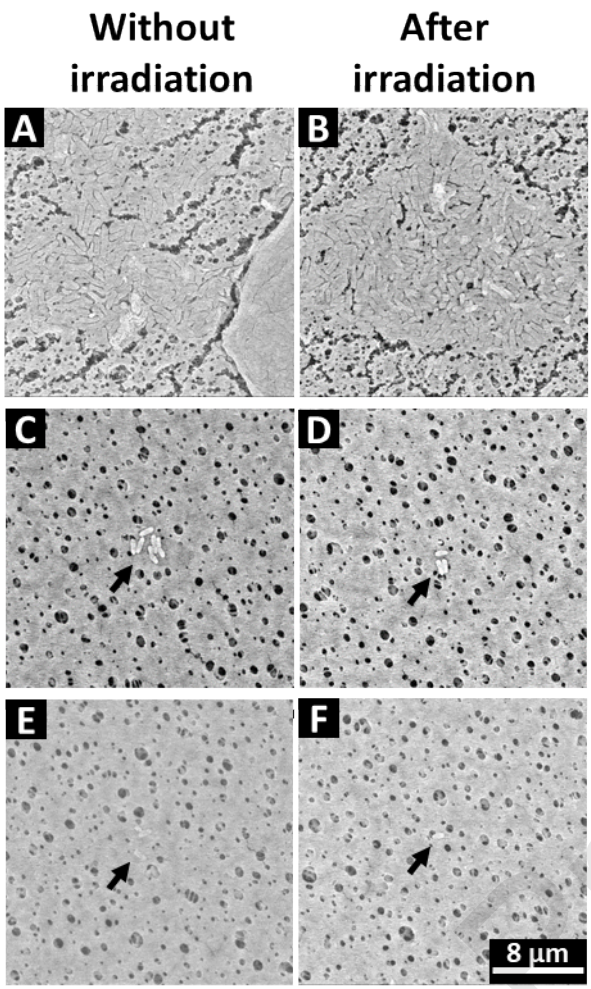

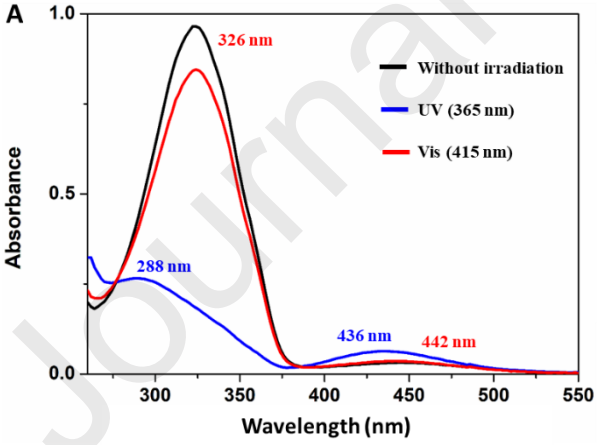

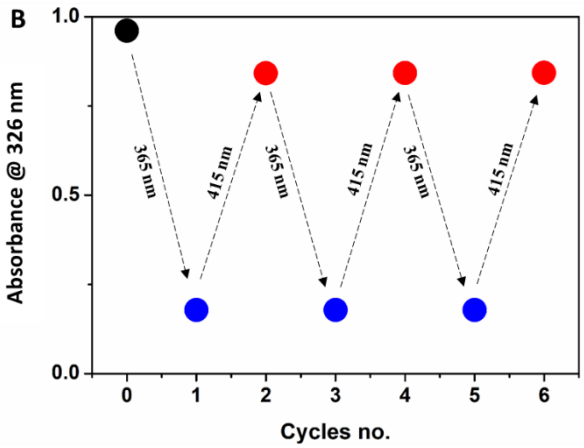

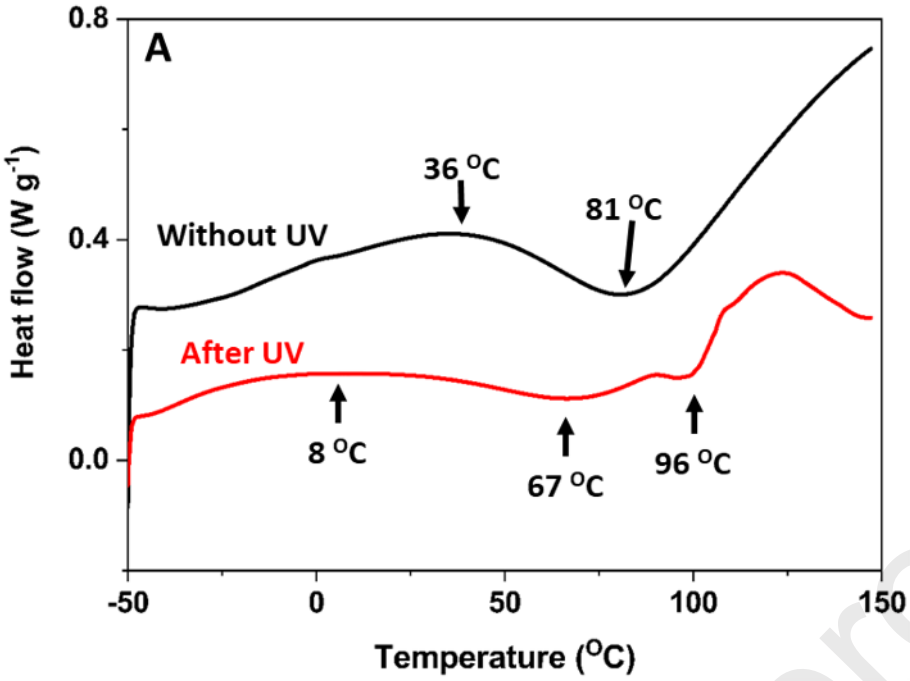

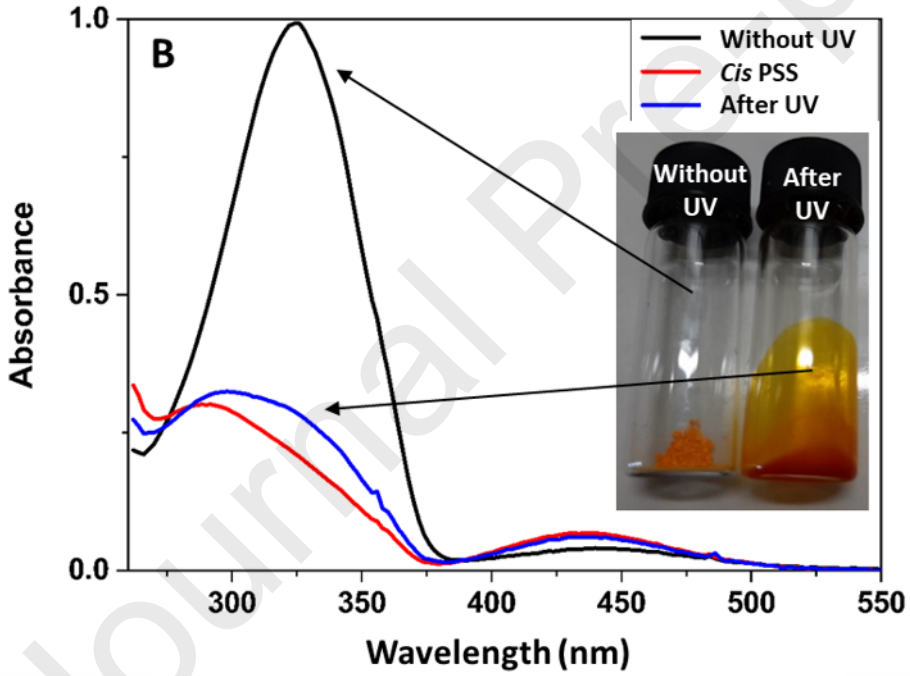

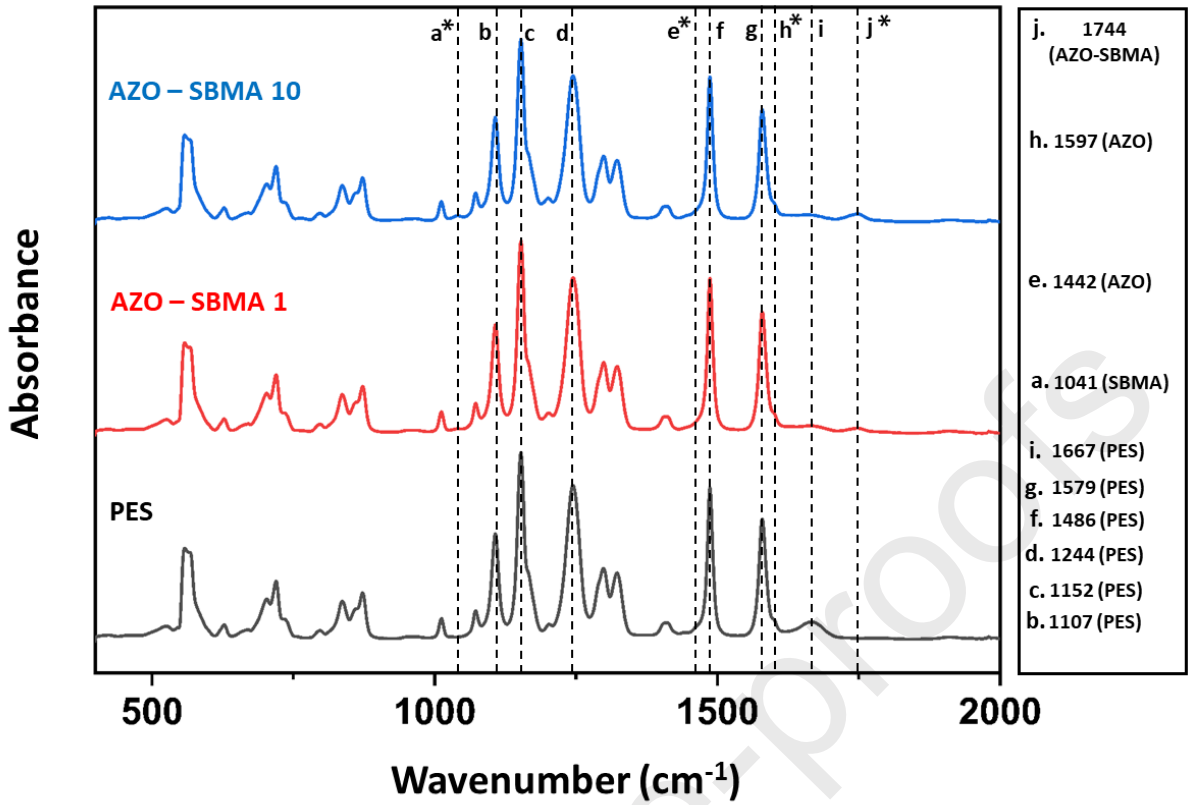

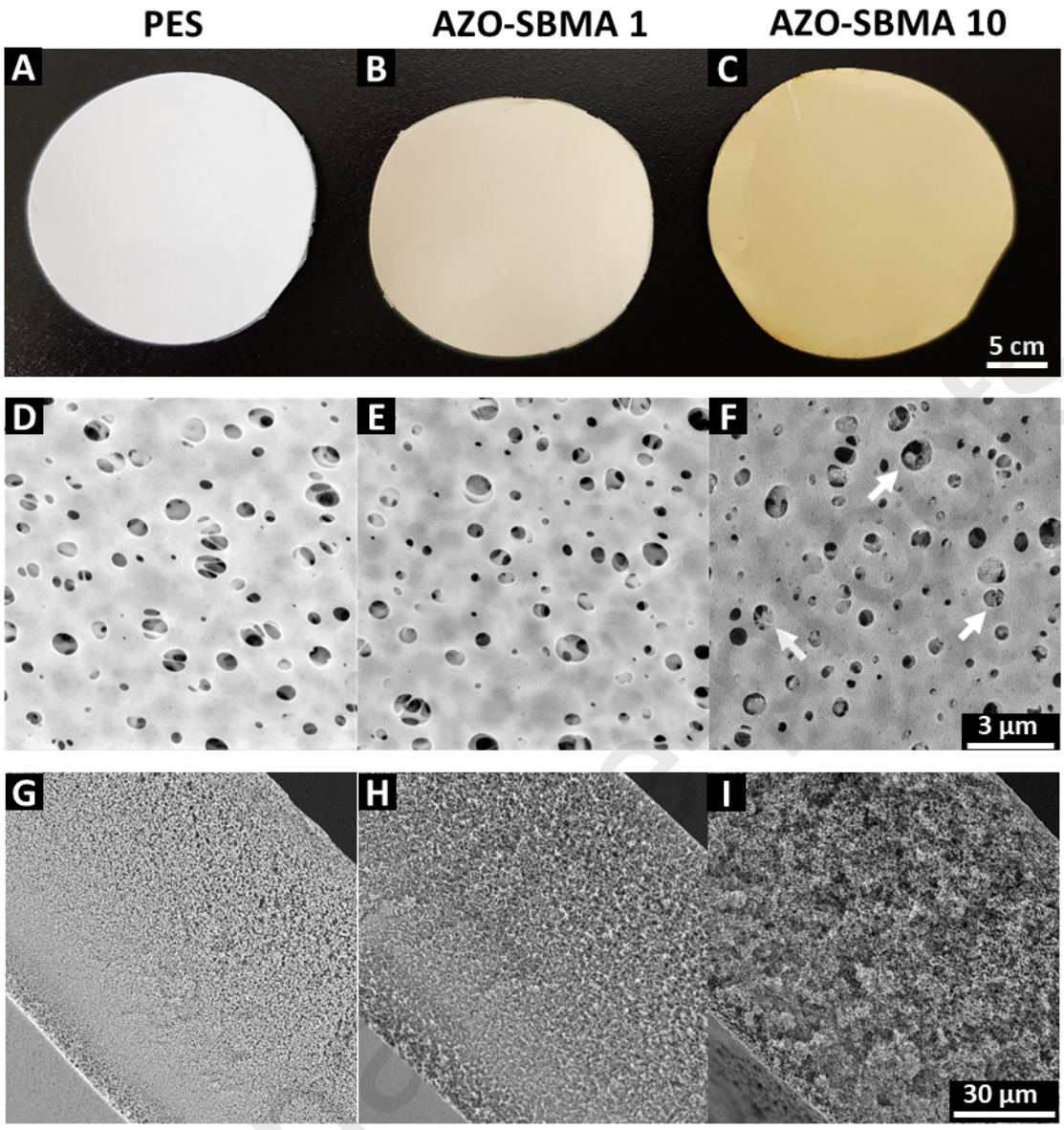
PES
AZO-SBMA 1
AZO-SBMA 10
A
B
C
5 cm
D
E
F
3 µm
G
H
I
30 µm